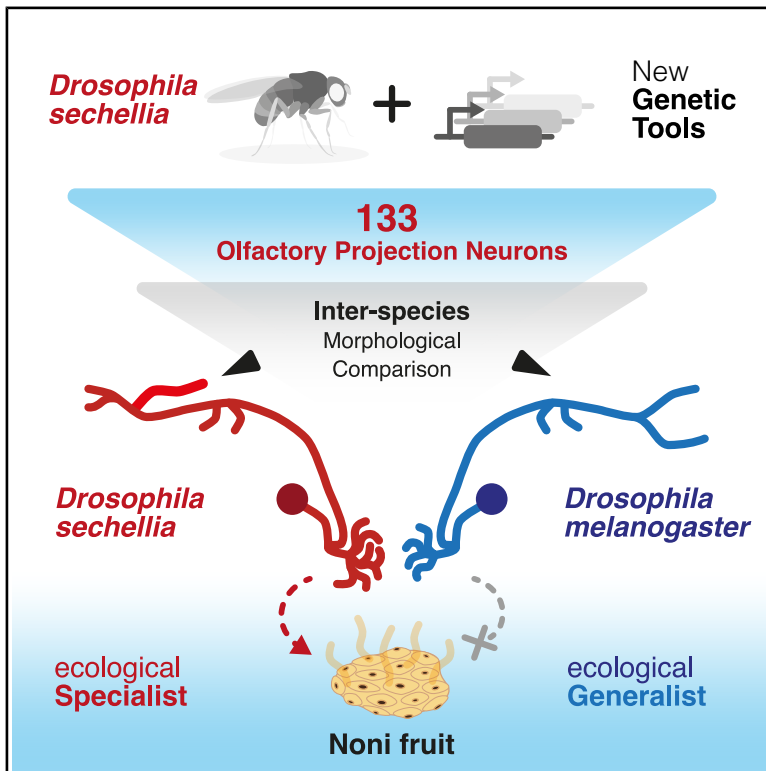


Cell Reports

Olfactory projection neuron rewiring in the brain of an ecological specialist

Graphical abstract



Authors

Benedikt R. Dür, Enrico Bertolini, Suguru Takagi, ..., Giovanna Lucarelli, Richard Benton, Thomas O. Auer

Correspondence

thomas.auer@unifr.ch

In brief

Dür et al. develop advanced genetic tools in the host specialist *D. sechellia* to study its olfactory system neuroanatomy. They show via single-cell labeling, tracing, and quantitative comparison of olfactory projection neurons with *D. melanogaster* that *D. sechellia* evolved specific anatomical changes in neurons linked to its unique host environment.

Highlights

- Genetic tools in *D. sechellia* facilitate comparative circuit studies
- An atlas of olfactory projection neurons' anatomy is created via stochastic labeling
- It highlights the re-wiring of specific cell populations linked to host odor detection



Resource

Olfactory projection neuron rewiring in the brain of an ecological specialist

Benedikt R. Dürr,^{1,2} Enrico Bertolini,^{1,3,4} Suguru Takagi,^{1,4} Justine Pascual,^{1,3,4} Liliane Abuin,¹ Giovanna Lucarelli,¹ Richard Benton,¹ and Thomas O. Auer^{1,3,5,*}

¹Center for Integrative Genomics, Faculty of Biology and Medicine, University of Lausanne, 1015 Lausanne, Switzerland

²Centre for Organismal Studies, Heidelberg University, 69120 Heidelberg, Germany

³Department of Biology, University of Fribourg, 1700 Fribourg, Switzerland

⁴These authors contributed equally

⁵Lead contact

*Correspondence: thomas.auer@unifr.ch

<https://doi.org/10.1016/j.celrep.2025.115615>

SUMMARY

Animal behaviors can differ greatly between closely related species. These behavioral changes are frequently linked to sensory system modifications, but central brain cell-type alterations might also be involved. Here, we develop advanced genetic tools to compare homologous central neurons in *Drosophila sechellia*, an ecological specialist, with the generalist *Drosophila melanogaster*. Through systematic morphological analysis of olfactory projection neurons (PNs), we reveal that the global anatomy of these second-order neurons is conserved. However, high-resolution, quantitative comparisons identify a striking case of convergent rewiring of PNs in two olfactory pathways critical for *D. sechellia*'s host location. Calcium imaging and labeling of pre-synaptic sites in these evolved *D. sechellia* PNs indicate that species-specific connections with third-order partners are formed. This work demonstrates that peripheral sensory evolution is accompanied by selective wiring changes in the central brain to facilitate ecological specialization and paves the way to compare other cell types throughout the nervous system.

INTRODUCTION

To prosper in defined ecological niches, animals exhibit specific behavioral programs matching their environmental requirements. Underlying these behaviors are neural circuits that receive external stimuli, integrate internal state, and control motor outputs. While behaviorally relevant circuits have been studied intensely in selected model species, the use of non-model organisms in comparative neuroscience is of growing interest.^{1–3} Technological advances in genetics and -omics methods facilitate the analysis of multiple species to address how behaviors evolve through the alteration of genes, molecules, cells, and circuits.^{4,5} Such comparisons help to detect hotspots of evolutionary change and decipher common principles of brain and circuit evolution.³

At the macroscopic level, the study of brain structures or number of cell types across large evolutionary timescales has uncovered examples of brain re-organization and divergence of cell numbers and types.^{6,7} At shorter evolutionary distances, circuit modifications across species through altered gene expression⁸ or cell-type composition,⁹ among other changes, are likely to be more subtle. However, comparing closely related species might provide insights into recent changes and help us to understand how the accumulation of small alterations can eventually impact circuit output.

Sensory systems, at the interface of the brain and the environment, are particularly prone to evolutionary adaptations¹⁰ and

have provided the few examples where anatomical insights at the single-cell level have been gained: Comparative connectomics after volumetric electron microscopy imaging has pinpointed anatomical changes in microcircuits in the vertebrate retina that impact signal processing.¹¹ Synaptic rewiring in feeding circuits of two nematodes is linked to divergent predatory behaviors.^{12,13} Similarly, in larval drosophilids, increased synaptic connections from the sensory periphery to shared downstream neurons explains the species-specific sensitivity of nociception.¹⁴ Although these limited examples demonstrate the promise of comparative connectomics, this approach is currently limited to small volumes and very small sample sizes.

The olfactory system in flies, with its well delineated neural pathways, is ideally suited to address the question of how individual circuits differ between species. This sensory system has a well-characterized, stereotypic neuroanatomy in *Drosophila melanogaster*^{15,16}. Olfactory information is sensed by olfactory sensory neurons (OSNs) located mainly in the antenna. OSNs project their axons into the antennal lobe (AL), where they ramify in distinct olfactory glomeruli and connect to projection neurons (PNs) and local interneurons. PNs then transmit olfactory information to higher brain areas, including the mushroom body (MB, a center for learning and memory) and the lateral horn (LH, involved in innate behaviors).¹⁷

The highly stereotyped nature of OSN-PN circuits has helped to uncover basic principles of neuronal differentiation, circuit



wiring, and processing of information in *D. melanogaster*. PN dendritic and axonal growth is orchestrated by transcriptional programs, which lead to coordinated development of connections between OSNs in the AL and downstream circuits.^{18–24} PNs from individual glomeruli project to distinct zones within the LH in a highly stereotypic manner across individuals. This suggests that LH targeting is hardwired and leads to a functional subdivision of the LH neuropil.

This stereotypic anatomy has a direct impact on the processing of olfactory information. Behaviorally relevant odorant valence is encoded by an odor-specific activation pattern of glomeruli in the AL,²⁵ ranging from single glomeruli to weighted summation of multiple pathways. After pre-processing at the OSN-PN synapse and integration of local interneuron inputs, information is transmitted by PNs to the MB and LH, where hedonic valences and odor intensities are represented as spatially segregated functional maps.²⁶ This spatial segregation helps to categorize odors based on their behavioral value^{27,28} and favors conversion of inputs onto downstream circuits with a defined behavioral role.

To understand how olfactory circuits evolve in response to changing environmental needs, *D. sechellia* is of particular interest: It is extremely specialized to life on a single host fruit, *Morinda citrifolia* (“noni”), compared to the closely related generalists *D. melanogaster* and *D. simulans* (Figure 1A). Specific amino acid changes in olfactory receptors (Or22a and Ir75b)^{29–32} increase *D. sechellia*’s sensitivity toward host odors, including methyl hexanoate (Or22a) and hexanoic acid (Ir75b) and are accompanied by increases in OSN number (Or22a, Or85c/b, Ir75b),^{33,34} which impact PN temporal response dynamics.³⁴ The Or22a and Or85c/b olfactory pathways seem to be particularly important for specialization of *D. sechellia* on its host fruit given their high sensitivity toward noni odors.^{29,33} In calcium imaging experiments, both display the highest relative activity among *D. sechellia* AL glomeruli compared to control odors like apple cider vinegar or responses in *D. melanogaster* upon noni encounter, which creates a relatively wide olfactory response.²⁹ Their central role for noni attraction is further supported by behavioral observations in wind tunnel and tethered-fly assays,^{29,34} where the respective mutants show a strong loss of attraction similar to that of mutants for the olfactory co-receptor Orco.²⁹

Despite the advances in understanding of peripheral olfactory evolution, we have very limited knowledge about relevant changes in central olfactory pathways.^{29,35} Laborious dye-filling and photoactivation experiments³⁵ suggest that there have been alterations in MB connectivity across species. However, obtaining single-cell resolution with these approaches is very challenging.

Given the direct link between circuit wiring, signal processing, and innate behaviors, we aimed to investigate how the neuroanatomy of individual olfactory PNs, connecting peripheral OSNs to the LH, has evolved lineage specifically in *D. sechellia*. To this end, we expanded the genetic toolset in *D. sechellia*^{29,34–37} to facilitate the comparative analysis of homologous circuits in the central brain at single-cell resolution. Our quantitative analysis of PNs between *D. sechellia* and *D. melanogaster* points toward specific rewiring of central brain circuits involved in olfactory behaviors. These results indicate

that anatomical rewiring and spatial re-organization of host cue-related inputs play an important role in olfactory signal processing and complement physiological and morphological alterations in peripheral sensory neurons.

RESULTS

Establishment of PN labeling tools in *D. sechellia*

To enable the comparison of homologous PN cell types in the central brain, we first developed several transgenic tools in *D. sechellia*. In *D. melanogaster*, libraries of promoter-Gal4 and split-Gal4 transgenes inserted at defined genomic locations^{38,39} have granted genetic access to numerous cell types.^{40–42} Genetic targeting offers the advantage over dye filling and photoactivation experiments^{31,35} that brain images from immunohistochemical staining can be registered on reference templates (established for all three species)^{29,43,44} for quantitative comparison of morphological alterations.⁴⁵ However, to achieve genetic labeling with high precision, site-directed transgenesis at multiple reliable locations in the genome is required to combine several transgenes in the same animal.

We previously found that a broad PN driver from *D. melanogaster* can work well when integrated into the *D. sechellia* white locus³⁴ (Figure 1B), but this site is disadvantageous because it disrupts the gene’s function in homozygosity (resulting in visually impaired flies). To establish other suitable landing sites, we introduced *attP* sequences into the *D. sechellia* genome via random piggyBac-integration and CRISPR-Cas9-mediated homologous recombination at the equivalent locations of well-characterized *attP* sites of *D. melanogaster* and *D. simulans* (JK22C,⁴⁶ *attP40*,⁴² *attP2*,⁴⁷ *su(Hw)attP2*,⁴⁸ *Dsim1029*⁴⁹) (Figures S1A and S1B; Table S1).

To assess these *D. sechellia* landing sites, we attempted the integration of a PN Gal4 transgene from *D. melanogaster*, *GMR86C10-Gal4*,⁵⁰ for two reasons: first, this driver is sparsely expressed in two PN populations (innervating VM5d and VM5v glomeruli²³) and thereby a more sensitive reporter of the (in) sensitivity of a landing site to genomic positional effects; second, the VM5d PNs receive input from OSNs expressing the receptors Or85c/b, which define a behaviorally important olfactory pathway.^{29,34} We succeeded in integrating the *GMR86C10-Gal4* driver into three different *attP* sites (*Dsec-white*, *Dsec-attP40*, and *Dsec-attP1029*; Table S2). When these drivers were combined with *UAS-effector* constructs, we observed faithful reproduction of the *D. melanogaster* expression pattern, labeling both VM5d and VM5v PNs in the *D. sechellia* brain (Figure 1C) for the latter two. However, the *attP* site at the white locus was more prone to ectopic background expression (Figure S1C). The transgenic labeling of VM5d in *D. sechellia* confirmed the expected 2- to 3-fold increase in size of this glomerulus^{29,34,51} and a change in its relative AL position toward the brain midline⁵¹ observed in previous studies.

To target PNs more sparsely and to prevent ectopic expression in other neurons, we turned to the split-Gal4 system.⁵² We selected the *VT033006-BD* (as the *VT033006-Gal4* transgene drives robust expression in PNs³⁴; Figure 1B) and *GMR72C11-AD* hemidriviers necessary for Gal4 reconstitution. In *D. melanogaster*, this enhancer combination labels PNs innervating the

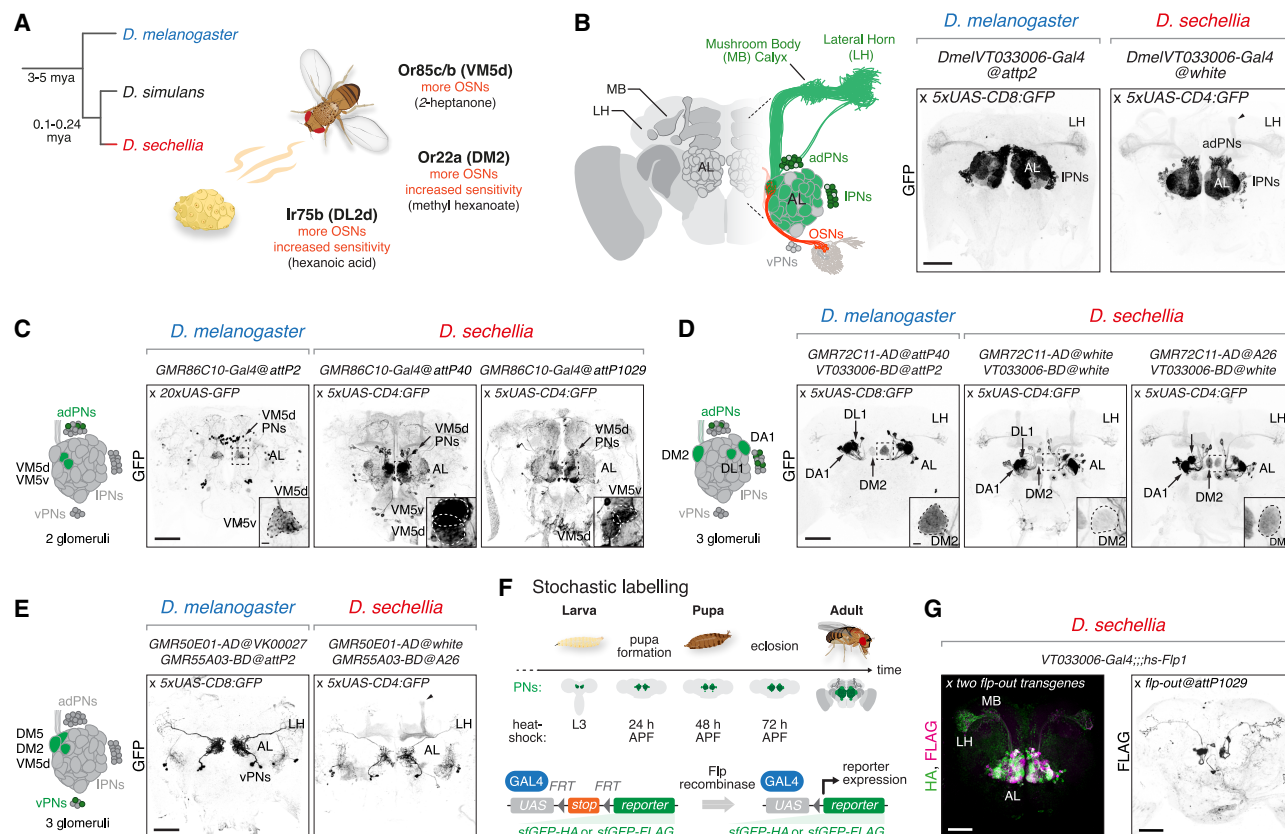


Figure 1. Generation of PN labeling tools in *D. sechellia*

(A) Phylogeny of *D. melanogaster*, *D. simulans*, and *D. sechellia*. The first two are cosmopolitan generalists; *D. sechellia* is an island endemic specialized on *Morinda citrifolia* ("noni") fruit which shows several changes in its peripheral olfactory system. Two olfactory pathways expressing receptors Or85c/b (whose axons project to the VM5d antennal lobe glomerulus) and Or22a (targeting DM2) are essential for long-range attraction to noni in *D. sechellia*, the Ir75b pathway (projecting to DL2d) is involved in egg laying.^{29,61} All three show increased OSN numbers in *D. sechellia*,³⁴ and the Ir75b or Or22a receptors show increased sensitivity to host volatiles^{29,31} (the main noni volatile activating each receptor is indicated).

(B) Left: schematic of the fly brain and the olfactory system. Olfactory sensory neurons (OSNs, orange) housed in sensilla on (mainly) the third antennal segment send axons to glomeruli in the antennal lobe (AL). Axons of neurons expressing the same receptor converge on the same glomerulus. Second-order PNs with cell bodies in three clusters (anterior-dorsal, ad; lateral, l; ventral, v) connect via their dendrites to OSNs and project axons to the mushroom body (MB) calyx and the lateral horn (LH). Right: anti-GFP immunohistochemical staining of central brains. The VT033006-Gal4 transgenic line labels ad- and l-PNs innervating 44 glomeruli.²⁴ Here and in other figures (if not indicated otherwise), brains were registered on a reference brain of the respective species (*D. melanogaster*: IS2, *D. sechellia*: DsecF).^{29,43} Black arrowhead: unspecific GFP expression in Kenyon cells (see Figure S1E). Scale bar, 50 μ m.

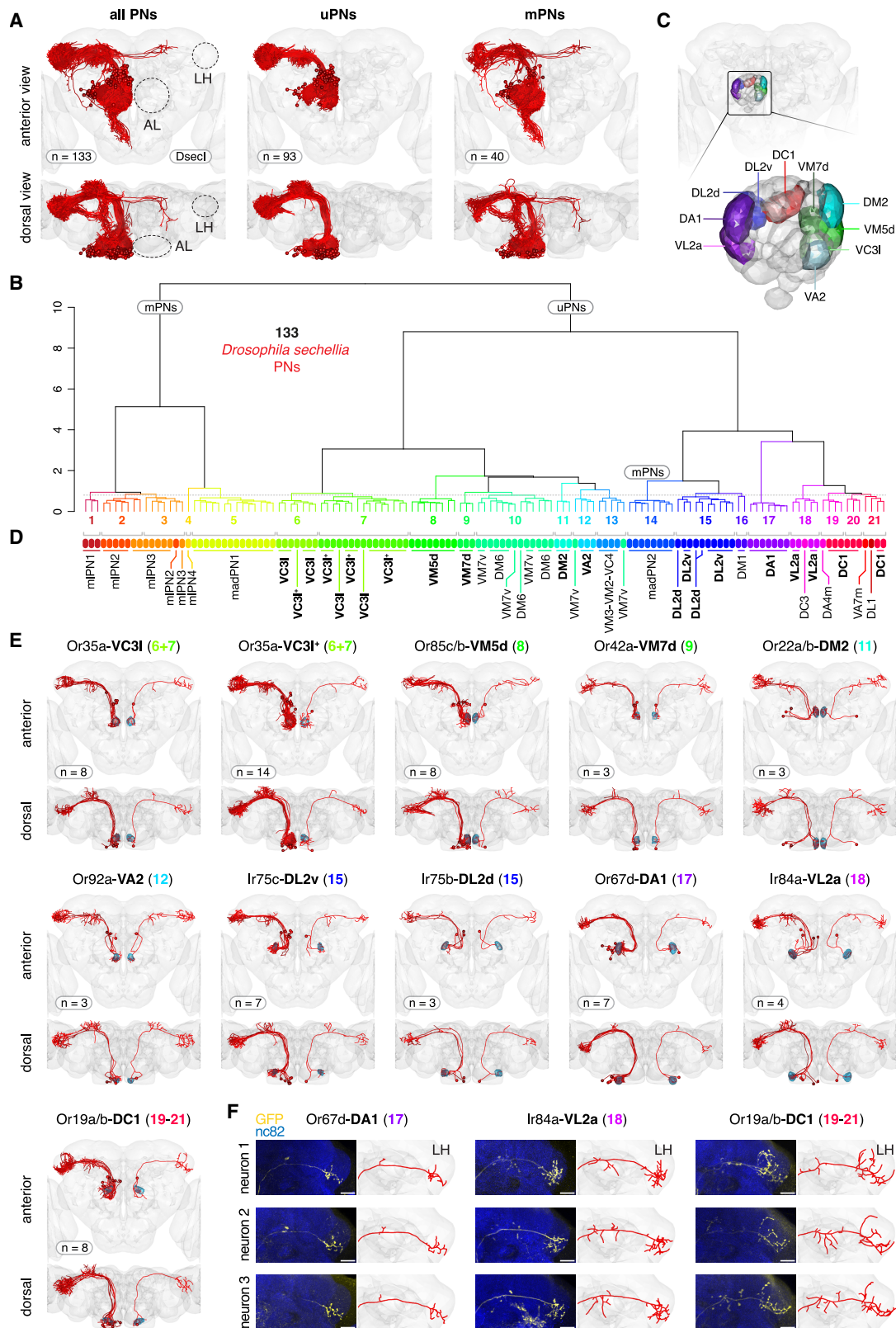
(C) Left: schematic of the AL highlighting glomeruli labeled by the transgenes shown on the right (same for D and E). Center: comparison of GMR86C10-Gal4-driven GFP expression in *D. melanogaster* and at two *D. sechellia* attP sites. Arrow: cell bodies of VM5d (and VM5v) PNs anterior-dorsal of the AL. The relative position of VM5d is more central in *D. sechellia* compared to *D. melanogaster*; its volume is 2.5-fold increased.²⁹ Sparse labeling of other brain cells in both species and some additional glomerular labeling were observed in *D. sechellia*. Scale bar, 50 μ m. Insets: AL glomeruli labeled by the respective transgene (same in D and E). Scale bar, 5 μ m.

(D) Labeling of the DM2, DA1, and DL1 glomeruli by a split-Gal4 combination in *D. melanogaster*. In *D. sechellia*, the integration of both hemidriviers at the same (center) or at different locations (right) leads to similar expression. Two to three additional glomeruli (asterisks) are weakly labeled by both combinations. Scale bar, 50 μ m.

(E) Split-Gal4 transgenics labeling ventral PNs (vPNs) with a complex dendritic branching pattern in the AL innervating DM2, DM5, and VM5d in *D. melanogaster* (center) and *D. sechellia* (right). Black arrowhead: unspecific GFP expression in Kenyon cells. Scale bar, 50 μ m.

(F) Schematics of the stochastic labeling approach. Top: timeline of PN development. The first adult PNs are specified in L3 larvae, and populations are added by neuroblast divisions during pupal development.⁵⁶ Indicated are time points of heat shock-mediated induction of Flp recombinase expression. Bottom: Flp recombinase mediates stop cassette excision and restores reporter expression (nonfluorescent superfolder sfGFP-HA or sfGFP-FLAG⁵⁵) in a few cells (see also Figure S2).

(G) Left: anti-FLAG and anti-HA immunofluorescence showing labeling of PNs in *D. sechellia* carrying two flip-out transgenes, the PN driver VT033006-Gal4 and a Flp recombinase source. Scale bar, 50 μ m. Right: anti-FLAG immunofluorescence of individual PNs in each brain hemisphere after Flp recombinase mediated cassette excision.



(legend on next page)

DM2, DA1, and DL1 glomeruli²⁴ (Figure 1D; SS01867). With our new transgenes in *D. sechellia*, we detected reproducible expression in all three glomeruli (Figures 1D and S1D). Integration of one hemidriver into another target site (*Dsec-attPpBac-A26*; to avoid transvection⁵³) (Figure 1D) resulted in a similar expression profile. Last, we tested a second hemidriver combination⁵⁴ (SS00587) specific for ventral PNs (not targeted by the reagents above), which led to comparable expression patterns across species (Figure 1E). In summary, we established a series of *attP* sites for site-directed transgenesis in *D. sechellia* (Table S3) and demonstrate that *D. melanogaster* enhancer constructs integrated at these locations can label homologous PNs in *D. sechellia*. All tested *D. melanogaster* enhancers showed similar expression in *D. sechellia*, indicating that their close phylogenetic relationship facilitates tool transfer. However, while all our attempts were successful, for other constructs and circuits, interspecific divergence in *cis*- and *trans*-regulation might require case-by-case evaluation.

While the split-Gal4 system offers a high degree of cell-type specificity, often no hemidriver combination exists for particular cell types or multiple cells are labeled. Therefore, we generated transgenic lines for stochastic cell labeling in *D. sechellia* based on Flp recombinase-mediated excision of a stop cassette (Figure 1F).⁵⁵ Using PNs as proof of principle for this approach offers several advantages. First, the stereotypic anatomy of the olfactory system enables identification of individual PNs and their probable presynaptic OSN partner based on their dendritic innervation pattern in the AL.^{19,20,56} Second, as PN somata are clustered in three groups around the AL neuropil, the soma position further supports classification into sub-populations.⁵⁶ Third, the extensive data on PN anatomy in *D. melanogaster* offers a unique opportunity to compare species.^{15,16,57}

We placed two FRT-reporter-transgenes (flip-out cassettes) through CRISPR-mediated integration at the location of two *attP* sites, *Dsec-attP40* and *Dsec-attP1029*, on two different chromosomes (II, III; Figures S1B and S2A). As a source of recombinase activity, we generated a transgenic line expressing Flp recombinase (Flp1⁵⁸) from a heat-shock promoter at the *Dsec-attPpBac-A26* site (chromosome IV) to combine all three transgenes without the need for recombination. To test these lines and to investigate the neuroanatomy of PN populations in *D. sechellia*, we sampled PN subtypes by combining our stochastic labeling tools with the broad *VT033006-Gal4* (Figure 1B) and *VT033008-Gal4* transgenes.³⁴ In transgenic animals carrying either both or a single flip-out cassette, we provided heat-shock induction of Flp1 after terminal differentiation

of PNs at late larval stages and during pupal development (Figure 1F), analogous to studies in *D. melanogaster*.^{18–20} For both transgene combinations, we generated PN-specific labels in female *D. sechellia* and isolated brains, where multiple or single PNs were labeled (Figure 1G). These new tools provide the opportunity to genetically target and reconstruct individual neuronal morphologies in *D. sechellia*.

Single-cell reconstruction of *D. sechellia* PN morphologies

To generate a comprehensive atlas of PN morphologies in *D. sechellia*, we dissected more than 800 brains. 620 of these showed strong reporter staining in PNs and the brain neuropil. We selected 184 brains with sufficiently sparse labeling to identify and fully trace individual PNs. We further filtered samples by requiring successful registration to a *D. sechellia* reference brain (generated by Auer et al.²⁹) so that traced cell morphologies could be compared in the same template. We obtained a dataset of 133 high-quality PNs in female *D. sechellia* from 117 different brains (Figure 2A). We manually traced the morphology of these PNs and annotated them depending on their dendritic branching pattern following the conventions established in *D. melanogaster*¹⁵: uniglomerular (uPNs), comprising uni- and uni⁺-PNs that innervate a unique glomerulus without or with some additional branches in other glomeruli, respectively, and multiglomerular PNs (mPNs), comprising oligo- and multiglomerular types that innervate several or the majority of glomeruli, respectively.¹⁵ In total, our dataset encompasses 93 uPNs and 40 mPNs (Figures 2A and S2B).

To provide additional categorization of *D. sechellia*'s PNs, we used NBLAST, which compares the morphological properties of traces and clusters them hierarchically.⁵⁹ Twenty-one distinct cell types emerged from this analysis (Figure 2B). To further improve this clustering-based characterization, we segmented AL glomeruli in the *D. sechellia* reference brain (based on Ellis et al.³⁵ and Depetris-Chauvin et al.⁶⁰) (Figure 2C) and used the dendritic innervation pattern of PNs to assign them to distinct AL glomeruli. In combination with the NBLAST output, this led to a refinement of our annotation, resulting in 26 distinct PN cell types in our *D. sechellia* dataset (Figures 2D and S2C).

Earlier studies in *D. melanogaster* have shown that PNs from individual glomeruli project to specific sub-regions of the LH and show a stereotypic branching pattern across animals.^{18–20} This morphology suggests that connectivity with downstream LH neurons and odor representation is conserved among individuals (and genetically hardwired, in contrast to PN-Kenyon

Figure 2. Identification of PN cell types in *D. sechellia*

(A) Right: 133 traced PNs registered on the *D. sechellia* Dsec1 reference brain. Center: 93 uniglomerular and uni⁺-glomerular PNs (uPNs). Left: 40 multiglomerular PNs (mPNs). Top: anterior view, bottom: dorsal view. A full list of all traced PNs is provided in Table S4.
(B) NBLAST clustering of the *D. sechellia* PN dataset results in 21 distinct clusters.
(C) *D. sechellia* reference brain with segmentation and annotation of AL glomeruli shown in (E).
(D) Manual curation of the 21 NBLAST clusters identifies 26 PN types. Colors indicate PN type; labels indicate the (main) innervated AL glomerulus. In bold: uPN types shown in (E). For VC3I, PNs with restricted innervation to VC3I or with additional innervations of other glomeruli (VC3I⁺) are shown.
(E) Eleven *D. sechellia* uPN types. Labels indicate the olfactory receptor expressed in OSN partners, the main innervated glomerulus (bold), and NBLAST cluster number (as in B). Left brain hemisphere: all neurons of the respective type in the *D. sechellia* dataset; right brain hemisphere: individual, representative neuron. Blue: segmentation of the AL glomerulus/glomeruli with main dendritic innervation. Sample size for each type is indicated.
(F) Anti-HA/GFP immunofluorescence of three representative Or67d-DA1, Ir84a-VL2a, and Or19a/b-DC1 PN axons (left) and the corresponding tracings (right) with stereotypic branching in the LH. Nc82 is a broad neuropil marker. Scale bar, 20 μ m.

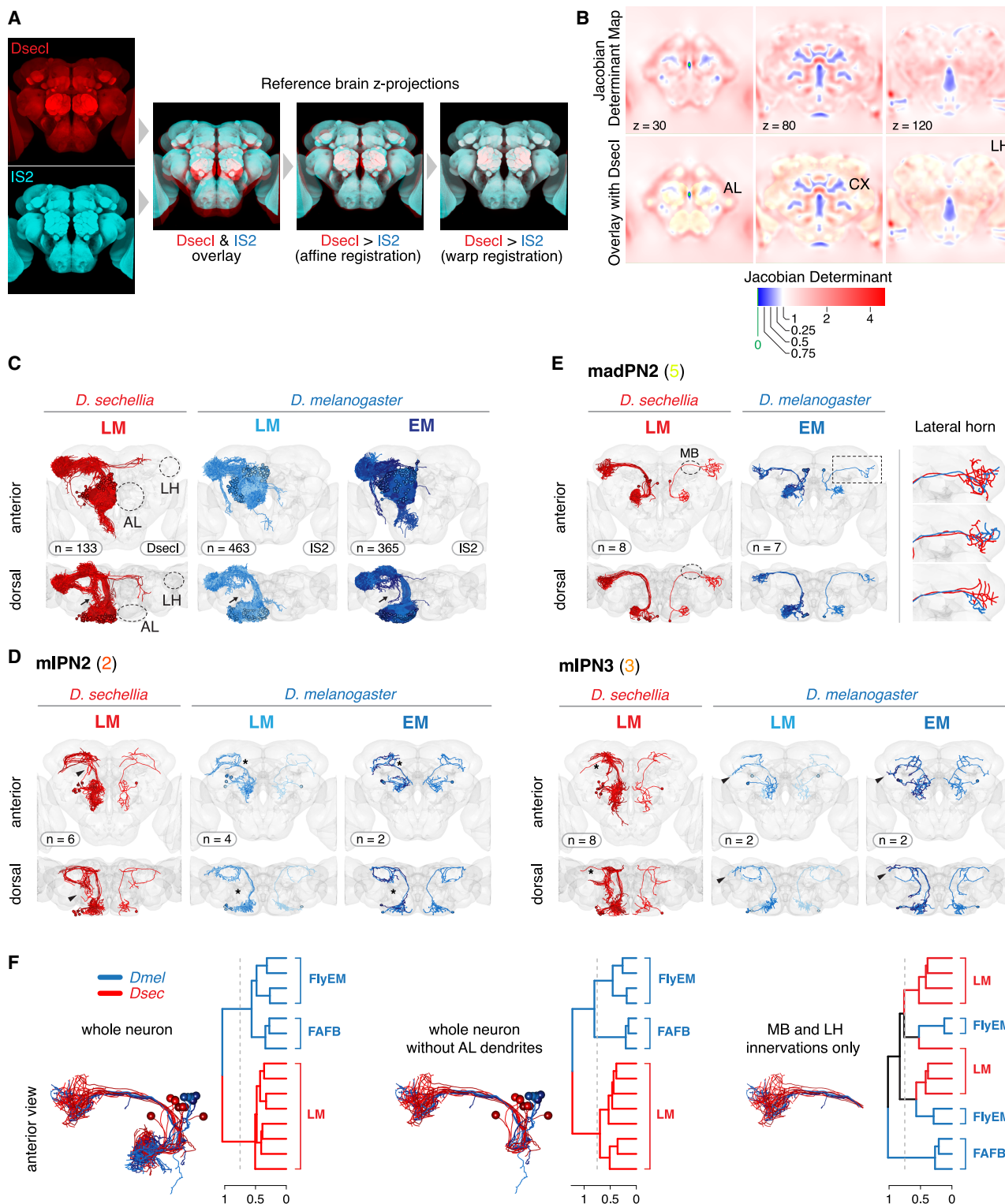


Figure 3. Comparison of *D. sechellia* and *D. melanogaster* brain and mPN morphologies

(A) Registration of the *D. sechellia* Dsecl reference brain (red) onto the *D. melanogaster* IS2 template (blue). Shown are the two reference brains (left), their overlay (center), and their overlay after affine (right) and after warp registration (far right).

(legend continued on next page)

cell connections in the MB that rather follow a stochastic connectivity pattern).³⁵ Comparing individual uPN neurons of the same type intraspecifically, we confirmed this stereotypy in LH branching exists also for *D. sechellia*'s PNs (Figures 2E and 2F), indicating that genetic hardwiring of cell morphology (and potential synaptic connectivity) among PNs is a conserved feature of these drosophilids.

The representation of PNs in our dataset was not uniform: For several PN types, we obtained only single representatives, while for others, we recovered up to 14 examples (Figure S2C). This bias might be caused by the genetic driver we used, which labels many but not all antero-dorsal and lateral PN populations. Moreover, the time window chosen for heat shocks (late larval and early pupal development; Figure 1F) might favor recombination in selected PN neuroblasts depending on their birth order.²⁴ Despite these caveats, the dataset contains a broad diversity of PN types with sufficient coverage to enable comparisons of the same cell type between species.

D. sechellia has evolved different PN morphology in noni-sensing pathways

Before comparing *D. sechellia* PNs to *D. melanogaster*, we investigated the similarity between the brain templates of both species. We calculated the Jacobian determinant¹⁹ for each voxel for the registration of the *D. sechellia* Dsecl reference brain into the *D. melanogaster* IS2 space to visualize the degree of deformation (expansion/contraction) within each brain area upon bridging registration (Figures 3A and 3B; Video S1). This showed that especially parts of the AL and the central complex diverge between both brains (probably because of the AL's location on the brain surface and the smaller inter-hemisphere space in Dsecl compared to IS2; Figure 3B). In the MB and LH area, however, we did not observe strong differences across brains, supporting the idea that PN arborizations can be quantitatively compared without registration artifacts (due to local deformation) after transfer of neuron reconstructions into the same brain space (Figures 3B and S3).

Next, we transferred PN reconstructions from *D. melanogaster* light imaging data (the Virtual Fly Brain⁵⁷) and two electron microscopy connectomes^{15,16} into the *D. melanogaster* IS2 space (Figure 3C). We limited our analysis to cell types of the ad- and l-PN clusters with at least three representatives within our *D. sechellia* dataset (19/26 cell types) to later systematically compare homologous cell types at single-cell resolution between species.

For the interspecific comparison between *D. melanogaster* and *D. sechellia*, we first focused on mPNs, which show complex cell morphologies and dendritic innervations of multiple AL glomeruli (Figures 3D and 3E). We identified five different mPN types in *D. sechellia*. Of these, the soma of three types are located in the l-PN cell cluster (we named them multi-lateral PNs 1–3, mLPNs1–3). Two of these mLPNs display alterations in their branching phenotypes in *D. sechellia* compared to *D. melanogaster* (mLPN2, mLPN3; Figure 3D); mLPN2s send more branches into anterior brain areas in *D. sechellia*, and mLPN3s instead show reduced branching in the LH in this species, with more pronounced projections toward the brain midline (Figures 3C and 3D). In the third type, mLPN1, morphology is comparable across species (Figure S4A).

The two cell types with antero-dorsal soma position, madPN1 and madPN2 (multi-antero-dorsal PN), show a similar overall branching pattern (Figures 3E and S4B). madPN2 neurons, which innervate the DL2d and DL2v glomeruli, form a more complex axonal arbor in the *D. sechellia* LH (Figure 3E). These neurons bypass the MB calyx without visible bouton formation (one branch was detected in one *D. melanogaster* neuron), indicative of only a minor role, if any, in associative learning. These neurons receive input from acid-sensing Ir75c and Ir75b OSNs, the latter of which directs species-specific oviposition site preference.⁶¹ The altered branching of this population in the LH could lead to differential weighting of acid-related cues in *D. sechellia* and have an impact on egg laying. To confirm the visually observed difference between *D. sechellia* and *D. melanogaster* neurons, we compared neuronal morphologies using interspecific NBLAST of all PN traces in the IS2 reference space (Figures 3F and S3A). In the resulting dendrogram, segregation into separate clusters could indicate either true biological difference in cell morphology, hemisphere-specific branching, or general dataset differences. To control for the latter two, beyond whole-neuron comparisons, we performed two pruning steps. First, we removed dendritic innervations in the AL to reduce the impact of altered AL morphology on clustering results. Second, we pruned neuronal axons until we were close to the MB to prevent the confounding effects of PN tract location (Figure 3F). Using this stepwise approach, *D. melanogaster* madPN2s formed a distinct cluster from those in *D. sechellia* using the first two types of neuron traces, and neurons did not segregate by either species or technique (Figure 3F). When using MB and LH innervations only, however, no species separation was observed any longer. This indicates that within madPN neurons

(B) Top: Jacobian Determinant Map indicates the degree of deformation for each brain area upon bridging registration from Dsecl to IS2. Shown are three focal planes highlighting the AL, central complex (CX), and LH (Video S1 shows the whole z-stack). Bottom: overlay with the Dsecl brain (yellow). Values >1 indicate expansion, values <1 indicate contraction, and zero indicates a collapsed voxel.

(C) Left: *D. sechellia* light microscopy (LM) dataset of 133 PNs (with soma in the ad- or l-PN cluster). Center: *D. melanogaster* LM dataset (from the Virtual Fly Brain⁵⁷) of 463 ad/l-PNs. Of these, 285 neurons were annotated and 178 lacked annotations. Right: *D. melanogaster* electron microscopy (EM) data^{15,16} of 365 ad/l-PNs (317 uPNs, 48 mPNs). Top: anterior view; bottom: dorsal view. Black arrow: increased anterior branching in mPNs of *D. sechellia* (see D).

(D) Two types of mPNs with cell soma in the lateral cell cluster (mLPNs) in *D. sechellia* (left) and *D. melanogaster* (center and right). mLPN2 display axonal branches reaching toward the anterior brain (arrows) only in *D. sechellia*; mLPN3s in *D. sechellia* show less branching into the LH (asterisk). Here and in the following panels, all neurons of a certain type are shown in the left hemisphere; a single, representative example neuron in the right hemisphere.

(E) mPNs with anterior-dorsal cell body position (madPN1) almost completely lack MB innervations and show complex axonal arbors in the *D. sechellia* LH (right: overlay in *Dmel* IS2).

(F) NBLAST clustering with either whole-neuron traces (left), traces lacking AL dendritic innervations (center), or only comprising the MB and LH branches (right). In the latter, *D. sechellia* (Dsec) PNs co-cluster with their *D. melanogaster* (Dmel) homologs.

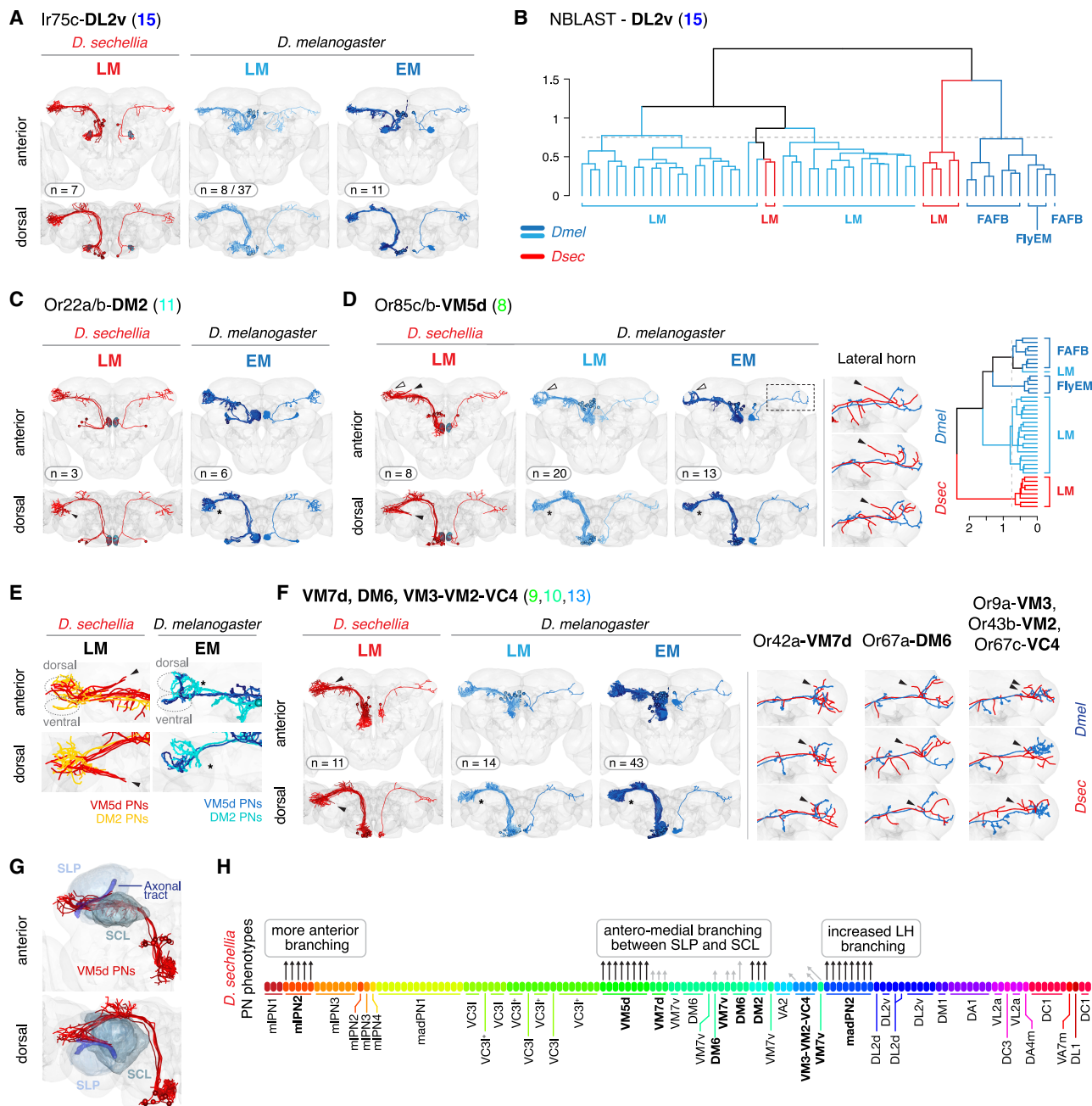


Figure 4. Comparison of *D. sechellia* and *D. melanogaster* uPN morphologies

(A) DL2v uPNs show a conserved morphology between both species (see Figure S4 for other PN types). Note that not all *D. melanogaster* neurons of (B) are visualized.

(B) NBLAST clustering using pruned axonal arbors does not separate *D. sechellia* DL2v PNs from their *D. melanogaster* homologs supporting the conserved neuroanatomy of this cell type (see Figure S3D for NBLAST results for whole-neuron traces and with partial trace pruning).

(C) Comparison of DM2 uPN morphologies between *D. sechellia* (left, LM) and *D. melanogaster* (right, EM) confirms published observations of additional antero-medial PN branching in *D. sechellia*²⁹ (arrowhead, absent in *D. melanogaster*: asterisk).

(D) VM5d PNs in *D. sechellia* (left) display a prominent antero-medial branch (black arrowhead) absent in *D. melanogaster* (asterisk) and branch less into the ventral LH area (white arrowhead). Right: three representative examples of LH branching of VM5d PNs in both species (overlay in *Dmel* IS2). NBLAST clustering using pruned axonal arbors separates *D. sechellia* (Dsec) PNs from their *Dmel* homologs (see Figure S3D for NBLAST results for whole-neuron traces and with partial trace pruning).

(E) Visualization of VM5d and DM2 PNs in *Dmel* IS2 for *D. sechellia* (left) and *D. melanogaster* (right). Indicated are the dorsal and ventral LH areas (circles). Arrowhead, antero-medial branching of both populations in *D. sechellia*, absent in *D. melanogaster* (asterisk).

(legend continued on next page)

similarly complex axonal arbours exist in *D. melanogaster*. As we cannot exclude that our genetic labeling approach consistently labels these complex neurons in *D. sechellia*, this result argues against a general species difference in all *D. sechellia* madPN2 neurons. However, the potential morphological variation in mPN is currently challenging to link to functional alterations in defined olfactory circuits as mPNs pool input from many OSN populations.

Therefore, we next focused on the morphology of (excitatory) uPNs that can be unambiguously identified by their dendritic AL innervations and which receive input from one main OSN partner.¹⁵ In eight uPN types, we did not detect any obvious morphological species differences (e.g., DL2v PN³¹; Figures 4A and 4B; NBLAST on pruned arbors), supporting the overall conserved anatomy of many PN types in *D. sechellia* (Figures S3D and S4C). Despite the broad conservation, however, we did detect several interspecific alterations. Consistent with previous work²⁹ *D. sechellia* DM2 PNs form an axonal branch, which is absent in *D. melanogaster*, leaving the densely packed LH area toward the antero-medial area of the brain (Figure 4C). The same antero-medial brain area is also innervated by multi-glomerular PNs in both species which form more projections in the anterior part of the brain in *D. sechellia* than in *D. melanogaster* (Figure 3A).

Notably, VM5d PNs display an even more prominent antero-medial branch, innervating the same brain region as DM2 PNs in *D. sechellia* (Figures 4D and 4E). Remarkably, while the overall axonal morphology of DM2 PNs within the LH is conserved between species, VM5d PNs display a clear reduction in their LH branching in *D. sechellia*. Detailed observation indicates that VM5d PNs maintain their innervation of the dorsal LH zone—restricted to olfactory inputs—while their branches in the ventral area, which receives multimodal input,^{15,16,62} is reduced (Figure 4D). NBLAST clustering using three differently pruned datasets of VM5d neuron traces supports a true species difference in the LH branching of this cell type (Figures 4D and S3D). The co-wiring of both PN populations out of the LH is particularly interesting as the cognate presynaptic sensory neuron partners of DM2 and VM5d PNs (Or22a and Or85c/b OSNs) are highly sensitive to noni odors, and both are involved in long-range attraction to the host fruit of *D. sechellia*.^{29,34}

The new antero-medial branch in both PN populations could therefore represent an additional evolutionary novelty in *D. sechellia* setting these two pathways further apart from other PN populations. To investigate this observation further, we performed photoactivation experiments in the antero-medial branch area in *D. sechellia* to label AL glomeruli innervated by PNs contributing to this structure. We found that DM2 and VM5d PNs, which are both located in the dorso-medial AL, were reverse labeled by this approach, further suggesting that these two populations are contributors to the *D. sechellia*-specific in-

nervations of this brain area (Figure S5A). Upon further inspection, we detected a few other PN types in *D. sechellia* (DM6, VM7v, VM7d, and VM2), which also display axonal processes in this same brain area with low frequency (3/8 in DM6, 2/6 in VM7v) or with a small antero-medial branch (VM7d, VM2) (Figure 4F). All these PN populations respond to food-related odors,⁶⁰ and their respective glomeruli are located in close proximity to DM2 and VM5d in the AL (Figure 5D). However, of all 11 uPN types sampled in our dataset, only DM2 and VM5d PNs consistently displayed novel projections into the antero-medial brain area.

To further characterize the target area of DM2 and VM5d PNs, we transferred anatomical segmentations from the Virtual Fly Brain to the IS2 space (Figure 4G). The *D. sechellia*-specific antero-medial PN branches elongate along an axonal tract between the superior clamp and the superior lateral protocerebrum. This tract is innervated by mPNs, MB output neurons, LH neurons, and others in *D. melanogaster* (see below) and represents a pre-defined exit point of the LH.

The co-registration of our *D. sechellia* PN dataset with existing traced neurons in *D. melanogaster* and our high-resolution analysis have revealed several morphological differences in mPN and uPNs. In support of a role in modified olfactory processing, we detected several instances of circuit rewiring in *D. sechellia* either in the LH (madPN2, VM5d) or toward a novel target area in the antero-medial brain innervated by olfactory pathways detecting noni odors (DM2 and VM5d) (Figure 4H).

***D. sechellia* VM5d PNs display differences in both axonal and dendritic wiring**

To confirm the novel antero-medial branching of VM5d PNs in *D. sechellia* with another genetic driver line, we made use of the *GMR86C10-Gal4* transgene (Figure 1C). This transgene allows the reproducible labeling of all VM5d PNs (eliminating any potential bias in our stochastically labeled neuron dataset). Using this independent driver, we again detected the novel antero-medial branching of VM5d PNs (Figure 5A). By combining this driver with our stochastic labeling tools, and using equivalent transgenes in *D. melanogaster*, we reconstructed additional VM5d PN morphologies in both species. All of these ($n = 7$) display a prominent antero-medial branch leaving the LH neuropil in *D. sechellia* which is absent in *D. melanogaster* (Figures 5B and 5C), further supporting the penetrance of this phenotype.

Within the AL, the VM5d glomerulus is more medially located and 2- to 3-fold larger in *D. sechellia* compared to *D. melanogaster* (Figure 5D).^{29,34,35,51,60} Upon closer inspection of VM5d dendritic branches in the AL of both species, we detected several instances of unexpected targeting in *D. sechellia*. VM5d PN dendrites frequently (in 4/7 examples) branched into the DM6, VM7d/v, VM2, or VC3 glomeruli (Figure 5E). In *D. melanogaster*, such targeting promiscuity was

(F) A few other uPNs show branching into the DM2/VM5d innervated antero-medial brain area in *D. sechellia* (arrowhead) absent in *D. melanogaster* (asterisk). Right: individual examples of VM7d, DM6, and VM3-VM2-VC4 uPN branching in the LH (overlay in *Dmel* IS2).

(G) Anatomical regions of the dorsal *D. melanogaster* brain. The *D. sechellia*-specific branch of VM5d PNs elongates along an axonal tract between the superior lateral protocerebrum (SLP) and the superior clamp (SCL).

(H) Summary of the observed PN morphological changes in *D. sechellia* compared to *D. melanogaster*. Arrows indicate whether individual neurons display the phenotype described on top. Arrow length indicates strength of phenotype (longer arrow, stronger phenotype; black arrows, 100% penetrance).

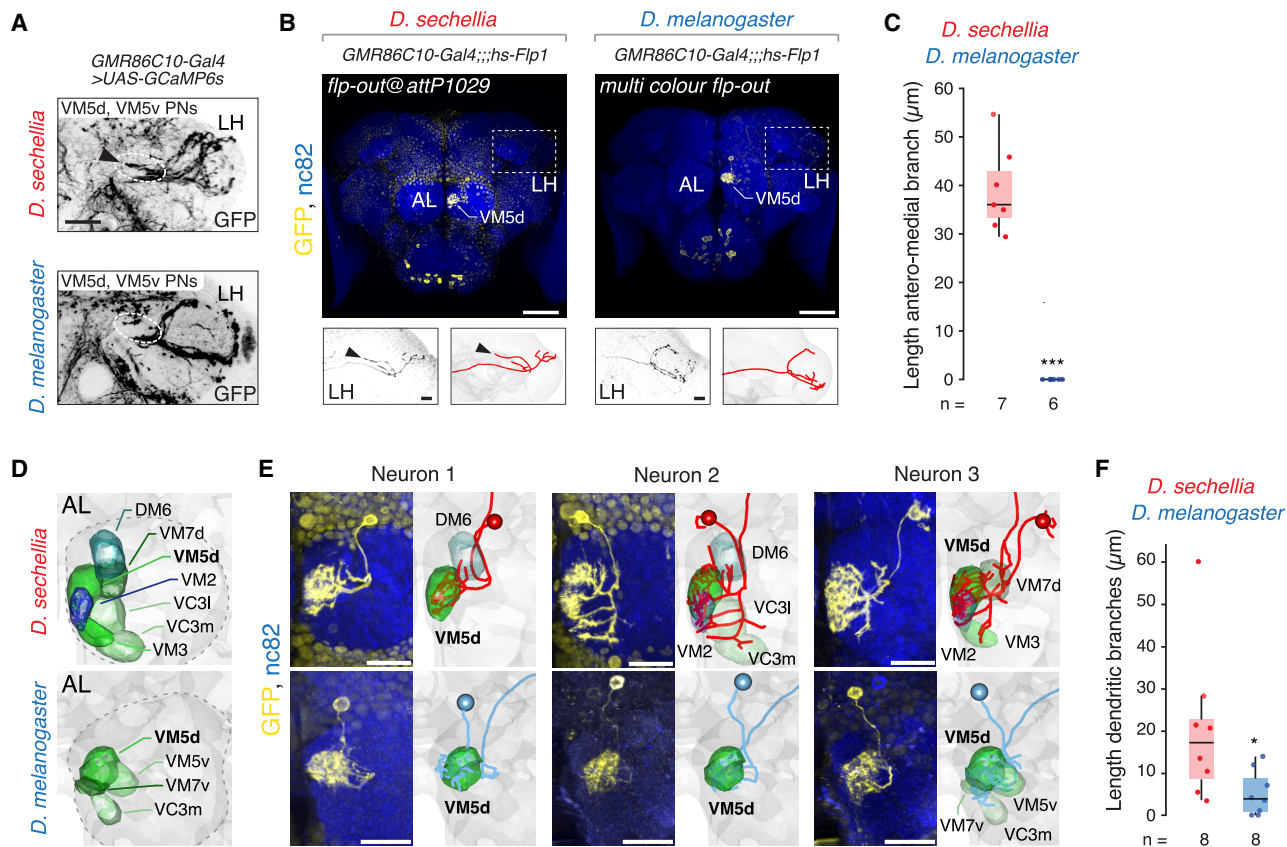


Figure 5. Novel axonal and dendritic branching in VM5d PNs

(A) Anti-GFP immunofluorescence showing the arborization of PNs in the GMR86C10-Gal4 transgenic line (Figure 1C) in *D. sechellia* and *D. melanogaster*. Circle and black arrowhead: antero-medial branch of VM5d PNs in *D. sechellia*. Scale bar, 20 μm .

(B) Anti-FLAG immunofluorescence in transgenic *D. sechellia* (left) and *D. melanogaster* (right) flies carrying flp-out reagents and the GMR86C10-Gal4 transgene. Scale bar, 50 μm . Bottom: axonal branching of one VM5d PN and neuron tracing. Arrowhead: antero-medial branch of VM5d PNs in *D. sechellia*. Scale bars, 10 μm .

(C) Quantification of VM5d PN antero-medial branch length ($n = 6-7$ females). For these and boxplots in (F), the center line represent the median, the box bounds represent the first and third quartiles, and whiskers depict at maximum $1.5 \times$ the interquartile range; individual data points are overlaid. Pairwise Wilcoxon rank-sum test, two-sided; *** $p < 0.001$.

(D) AL segmentation of selected glomeruli neighboring VM5d in *D. sechellia* (top) and *D. melanogaster* (bottom).

(E) Left: anti-FLAG immunofluorescence of individual VM5d PNs in the *D. sechellia* (top) or *D. melanogaster* (bottom) AL. Right: Reconstruction of the dendritic arbor of the stained neuron is shown on the left and VM5d and other innervated glomerular boundaries. Scale bar, 20 μm . Three neurons/species.

(F) Quantification of VM5d PN dendritic branch length outside the VM5d glomerulus ($n = 8$ females). Pairwise Wilcoxon rank-sum test, two-sided; * $p < 0.05$.

not detected, with VM5d PNs showing minor dendritic innervations of VM7d or VC3m only in few cases (2/6) and overall shorter branch length outside the VM5d glomerulus (Figure 5F). Intriguingly, the glomeruli innervated by *D. sechellia* VM5d PNs are the same as those whose PNs show occasional axonal antero-medial branching and co-wiring with VM5d PNs. In summary, this PN type displays both axonal and dendritic wiring alterations in *D. sechellia*.

Antero-medial PN axon targeting is a *D. sechellia*-specific, recessive trait

We next wanted to clarify whether the novel antero-medial branches of DM2 and VM5d PNs are *D. sechellia* specific and therefore turned to its closest relative *D. simulans*. To visualize PNs in this species, we generated a *D. simulans* VT033006-Gal4 line and combined it with a fluorescent reporter.⁶³ We

imaged the LH and adjacent brain regions and compared PN innervation patterns across all three species. Only *D. sechellia* showed staining in the area antero-medial to the LH (Figure 6A). Next, we expressed photoactivatable GFP³⁵ in *D. simulans* pan-neuronally. Following specific activation of the VM5d glomerulus in *D. simulans*, we detected no branches reaching into the antero-medial brain area next to the superior clamp, as seen in *D. sechellia* (Figure S5B).

To gain insights into the genetic architecture of the *D. sechellia*-specific antero-medial PN branching, we analyzed PNs in *D. sechellia*/*D. simulans* and *D. sechellia*/*D. melanogaster* hybrids. In both hybrid combinations, no *D. sechellia*-like branching phenotype is detected (with a minimal branch observed in the *D. sechellia*/*D. simulans* hybrids in 2/6 cases) (Figure 6B). Consistent with this result, in interspecific hybrids

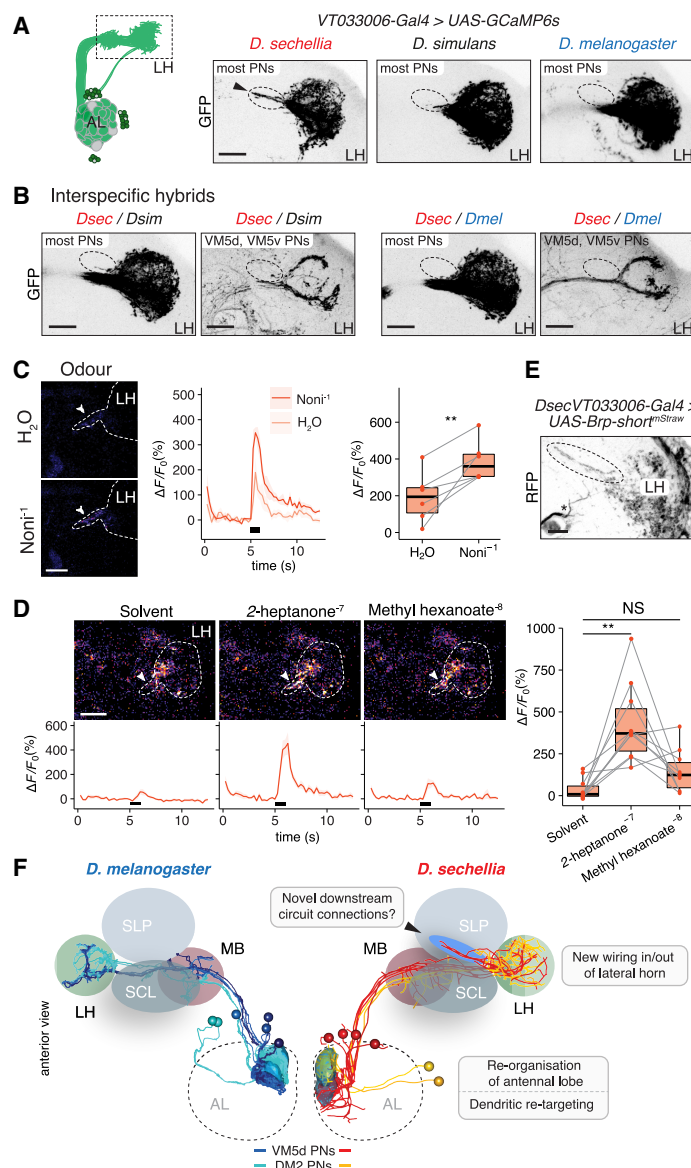


Figure 6. Genetic basis and activity of *D. sechellia*-specific PN branches

(A) Left: schematic of labeled PNs. Right: anti-GFP immunofluorescence in VT033006-Gal4, UAS-GCaMP6s transgenics. Only in *D. sechellia* axonal branching from the LH toward the antero-medial part of the brain is detected (midline to the left).

(B) Anti-GFP immunofluorescence showing PN branching of transgenic interspecific hybrids expressing VT033006-Gal4, UAS-GCaMP6s (left) or GMR86C10-Gal4, UAS-GFP (right). Left: *D. sechellia*/*D. simulans* hybrids. Right: *D. sechellia*/*D. melanogaster* hybrids. No *D. sechellia* equivalent antero-medial branch in VM5d or other labeled PNs is detected (circle). Scale bars, 20 μ m.

(C) Left: odor-evoked neuronal activity in the *D. sechellia* antero-medial PN branch in VT033006-Gal4, UAS-GCaMP6f transgenic animals upon presentation of water and noni juice (at 10⁻¹ dilution). White arrow: branch area quantified. Scale bars, 25 μ m. Center: relative increase in fluorescence ($\Delta F/F_0$) in percentage upon stimulus presentation. Black bar, stimulation window. Right: maximal responses toward each stimulus ($n = 6$ females). For these and boxplots in (D), the center line represents the median, the box bounds represent the first and third quartiles, and whiskers depict at maximum 1.5 \times the interquartile range; individual data points are overlaid. Paired t test, two-sided; ** $p < 0.01$.

(D) Odor-evoked neuronal activity in the *D. sechellia* antero-medial PN branch in VT033006-Gal4, UAS-GCaMP6f transgenic animals upon presentation of solvent (dichloromethane), 2-heptanone⁻⁷, or methyl hexanoate⁻⁸. The latter two specifically activate VM5d and DM2 PNs at the given concentration.³⁴ White arrow: branch area quantified. Scale bar, 25 μ m. Bottom: relative increase in fluorescence ($\Delta F/F_0$) in percentage upon stimulus presentation. Right: maximal responses toward each stimulus ($n = 10$ females). Paired t test, two-sided; ** $p < 0.01$; NS = $p > 0.05$.

(E) Expression of a *Brp-short*^{mStraw} transgene in *D. sechellia* PNs reveals labeling of potential pre-synaptic sites in the antero-medial branch area (in circle). Asterisk, unspecific labeling. Scale bar, 10 μ m.

(F) Summary of anatomical differences in the AL-LH circuitry between *D. melanogaster* and *D. sechellia*. Shown are four VM5d and two DM2 PNs in both species. *D. sechellia* shows a re-organization of its AL glomeruli positions and dendritic re-targeting in VM5d PNs. In the LH, fewer axonal branches are present in the ventral part with antero-medial branches (arrowhead) exiting the LH (and co-wiring of VM5d and DM2 PNs), potentially forming novel connections with downstream partners.

in which VM5d/VM5v PNs were labeled using the GMR86C10-Gal4 driver, no antero-medial branch was present (Figure 6B). Collectively, these experiments suggest that altered PN axonal branching into the antero-medial brain is a derived, recessive trait in *D. sechellia*.

Noni odor-evoked activity is transmitted to a new target area

To test whether the *D. sechellia* DM2 and VM5d antero-medial PN branches transmit noni odor-evoked activity, we performed 2-photon calcium imaging using the broad PN driver VT033006-Gal4 coupled with UAS-GCaMP6f while presenting animals with olfactory stimuli. We observed a robust noni response in *D. sechellia* in the antero-medial branch area, compared to water control (Figure 6C). This result supports that food-related olfactory signals converge into this target

area and are potentially transmitted to downstream partners. To monitor the individual contribution of VM5d and DM2 PNs populations to the observed activity, we used as stimulants low concentrations of 2-heptanone and methyl hexanoate, which mainly activate Or85c/b (VM5d) and Or22a/b (DM2) sensory neurons, respectively.³⁴ For both stimuli, we could detect activity in the *D. sechellia*-specific branching area (Figure 6D); this activity was weaker for the Or22a/b-specific odor, consistent with the less-prominent innervation of DM2 PNs compared to VM5d PNs.

Finally, we labeled synaptic active sites in these neurons using a UAS-Brp-short^{mStraw} transgene.⁶⁴ Like axons within the LH, the antero-medial PN branches show distributed punctate staining throughout their whole length (Figure 6E). This result suggests that pre-synaptic sites are established within these branches, consistent with them forming functional synapses

with downstream neurons (see discussion). Together with the above physiological results, these experiments support our anatomical data and indicate that noni-responsive pathways form *D. sechellia*-specific connections in the antero-medial brain and suggest that they have functional relevance for the interpretation of noni odors in downstream circuits.

DISCUSSION

We have used two closely related, genetically accessible fly species as a paradigm to understand principles of neural circuit evolution. Using a suite of genetic tools, we were able to genetically compare more than 20 homologous cell types in the central brains of multiple individuals. Olfactory PNs are ideally suited for this approach as they are critical for olfactory processing and can be unambiguously identified through their stereotypic wiring.

The *attB/attP* system that we have employed offers the advantage that published constructs of *D. melanogaster* can be re-used to label homologous cell types across the *D. melanogaster/D. simulans/D. sechellia* trio. The four *attP* sites described here, located on each of the four chromosomes, allow the combination of up to four transgenes without the need for recombination. Future efforts will be necessary to transfer other markers into *D. sechellia* to facilitate the creation of more complex genotypes.

Our analysis of PN morphologies across *D. melanogaster* and *D. sechellia* revealed that while most cell types exhibit a conserved interspecific morphology, modifications in mPNs and uPNs exist. In particular, the axonal rewiring of the DM2 and VM5d PN populations in *D. sechellia* is intriguing as both pathways are involved in long-range attractive behavior toward noni.^{29,34} These neuron types are developmentally not closely related—deriving from distinct neural stem cell lineages⁵⁶—and the specificity of the antero-medial branch for those two cell types implies that anatomical convergence is an adaptive trait selected by their common function in noni detection. While there is no specific evidence for increased axonal-axonal synaptic contacts between both populations in *D. melanogaster*,¹⁵ these might be present in *D. sechellia* as axon-axon proximity strongly relates to the number of synapses between cells.⁶⁵ Querying the *D. melanogaster* connectome, beyond mPNs, many other neurons innervate the antero-medial branch area, including those of the superior lateral, medial, and intermediate protocerebrum, MB output neurons, and LH neurons (LHNs) (Figure S6; Table S5). The latter represent excellent candidates for novel connections in *D. sechellia* as they show stereotypic odor responses across animals in *D. melanogaster*^{27,28} and receive on average excitatory input from 6 to 7 PNs.^{15,16,28} As we sampled PNs across many brains in *D. sechellia*, it is unclear how many PNs innervate the *D. sechellia* antero-medial branch area per animal. However, the number of DM2 and VM5d PNs per hemisphere (2 and 4, respectively), together with occasional innervations of other PN types (e.g., DM6, VM7d), match well with the anticipated average input per LHN. In *D. melanogaster*, LHNs are better odor categorizers than individual PNs and stereotypically pool-related inputs^{27,28}; *D. sechellia* LHNs receiving input from the antero-medial PN branch might therefore process noni as a highly ecologically relevant odor mixture (Figure 5F).

Previous work in *D. melanogaster* PN development has shown that axonal and dendritic wiring is controlled by common regulatory networks.⁶⁶ In the case of VM5d, where axonal branching in the central brain and dendritic targeting in the AL are modified in *D. sechellia*, both could have a common genetic basis. Recently developed methods to study PN wiring^{21–24} will be instrumental to investigate how species-specific wiring can be established during development. The re-location of VM5d in the *D. sechellia* AL and dendritic innervation of neighboring glomeruli could allow pooling of food-related inputs into a single pathway, although we cannot exclude that this has no adaptive function. Until now, response properties in these PNs have been sampled only with a single odorant.³⁴ It will be interesting to test whether targeting promiscuity in *D. sechellia* impacts physiological VM5d PN response properties, for example, by broadening their response profile.

Overall, the genetic toolset presented here opens the door for more sophisticated genetic manipulations in drosophilids. Comparative studies in homologous mating circuits underlying species-specific behaviors^{63,67–72} can build on this approach to delineate neuroanatomical species differences deep inside the brain. In combination with connectomic reconstructions after volumetric electron microscopy imaging,^{15,16} it represents a powerful way to identify novel circuit motifs and their plasticity across individuals. In *D. sechellia*, other phenotypic traits like modified gustation,⁷³ oviposition,⁶¹ metabolism,^{74–76} immune response,⁷⁷ sleep,⁷⁸ circadian rhythms,⁷⁹ song production,⁶⁸ or walking⁸⁰ will benefit from the reagents presented here. Sampling closely related species points toward the accumulation of several changes in few pathways, from the periphery to the central brain, and studies in other selected drosophilids with diverse phenotypes and evolutionary relatedness will help to detect recurrent evolutionary novelties. Insights from such work will likely be relevant to inform how brains of all animals adapt to changing environments.

Limitations of the study

In the present study, we did not systematically test the established *Dsec attP* sites with enhancer-Gal4 drivers targeting diverse circuits. More detailed studies will be required to evaluate *cis*-regulatory input at each target locus. In addition, while our results indicate that *D. melanogaster* sequences can label homologous neuron types in *D. sechellia*, *cis*- and/or *trans*-regulatory evolution might require species-specific reagents and careful evaluation of labeled cell types. Our light imaging-based neuron reconstruction approach suffers from potential low-level labeling and inability to capture fine processes under confocal microscopy. Having sampled 133 PNs representing 26 types, the current *D. sechellia* dataset is not exhaustive, and additional efforts will be required to gain a complete overview of the olfactory PN connectome of this species.

RESOURCE AVAILABILITY

Lead contact

Further information and requests for resources and reagents should be directed to and will be fulfilled by the lead contact, Thomas O. Auer (thomas.auer@unifr.ch).

Materials availability

All unique biological materials generated in this study (e.g., mutants, plasmids, transgenic fly strains) are available from the lead author upon request.

Data and code availability

- All raw imaging data have been deposited at Zenodo as <https://doi.org/10.5281/zenodo.15002759> and are publicly available as of the date of publication.
- All original code has been deposited at GitHub (<https://github.com/AuerTomLab/Duerr2025>) and Zenodo and is publicly available at <https://doi.org/10.5281/zenodo.15012945> as of the date of publication.
- Any additional information required to reanalyze the data reported in this paper is available from the [lead contact](#) upon request.

ACKNOWLEDGMENTS

We thank David Stern, David O'Brochta, Iris Salecker, Stephan Sigrist, Benjamin Prud'homme, Sophie Caron, Gerald Rubin, Yoshi Aso, Heather Dionne, the Bloomington *Drosophila* Stock Center (NIH P40OD018537), and the Developmental Studies Hybridoma Bank (NICHD of the NIH, University of Iowa) for sharing reagents; Yoshi Aso and Greg Jefferis for pointing us to enhancer-Gal4 and split-Gal4 combinations; Alexander Bates, Philipp Schlegel, and Sebastian Cachero for help with natverse; and Felix Meyenhofer for help with Jacobian determinant visualization. We also thank Ana Depetris-Chauvin and Silke Sachse for sharing their *Drosophila sechellia* AL segmentation prior to publication; Anabela Rebelo Pimentel for help with embryo alignments for microinjections; Roman Arguello, Gáspár Jékely, and Anne von Philipsborn for comments on the manuscript; and Gáspár Jékely for support to B.R.D. This work was supported by a Deutsche Forschungsgemeinschaft Walter-Benjamin Fellowship (E.B.); a Marie Skłodowska-Curie Actions Individual Fellowship (836783), an EMBO Long-Term Fellowship (ALTF 454-2019), and a Japanese Society for the Promotion of Science Overseas Research Fellowship (202360258) (S.T.); the University of Lausanne, the Swiss National Science Foundation (SNSF) (310030B-185377 and 310030_219185), European Research Council Consolidator (615094), and European Research Council Advanced (833548) grants (R.B.); and an SNSF Ambizione (PZ00P3185743) and Starting Grant (TMSGI3_211391/1), the Fondation Pierre Mercier pour la Science, the Novartis Foundation for Biomedical Research, and the University of Fribourg (T.O.A.).

AUTHOR CONTRIBUTIONS

T.O.A. conceived the project. All authors contributed to experimental design, analysis, and interpretation of results. The specific experimental contributions were as follows: B.R.D. performed immunostainings and tracings and analyzed all PN morphological data. E.B. mapped transgenic insertion sites and performed molecular cloning. S.T. performed the photoactivation and calcium imaging experiments. J.P. performed immunostainings, helped with molecular cloning, and maintained transgenic fly strains. L.A. performed molecular cloning and helped with line establishment. G.L. helped with micro-injections and maintained transgenic fly strains. R.B. provided guidance throughout the project. T.O.A. performed molecular cloning, immunostainings, and generated transgenic lines and wrote the paper, with input from all authors. T.O.A. and B.R.D. prepared the figures. All authors approved the final version of the manuscript.

DECLARATION OF INTERESTS

The authors declare no competing interests.

STAR★METHODS

Detailed methods are provided in the online version of this paper and include the following:

- [KEY RESOURCES TABLE](#)
- [EXPERIMENTAL MODEL DETAILS](#)
 - *Drosophila* husbandry

METHOD DETAILS

- *Drosophila* microinjections
- Molecular cloning
- Insertion site mapping
- Flip-out mediated stochastic labeling
- Immunohistochemistry
- Image acquisition and processing
- *In vivo* two-photon calcium imaging and photoactivation

QUANTIFICATION AND STATISTICAL ANALYSIS

SUPPLEMENTAL INFORMATION

Supplemental information can be found online at <https://doi.org/10.1016/j.celrep.2025.115615>.

Received: August 16, 2024

Revised: December 24, 2024

Accepted: April 3, 2025

REFERENCES

1. Laurent, G. (2020). On the value of model diversity in neuroscience. *Nat. Rev. Neurosci.* 21, 395–396.
2. Averof, M., and Sinigaglia, C. (2020). Introduction to emerging systems. *EvoDevo* 11, 8.
3. Jourjine, N., and Hoekstra, H.E. (2021). Expanding evolutionary neuroscience: insights from comparing variation in behavior. *Neuron* 109, 1084–1099.
4. Roberts, R.J.V., Pop, S., and Prieto-Godino, L.L. (2022). Evolution of central neural circuits: state of the art and perspectives. *Nat. Rev. Neurosci.* 23, 725–743.
5. Tosches, M.A. (2017). Developmental and genetic mechanisms of neural circuit evolution. *Dev. Biol.* 431, 16–25.
6. Herculano-Houzel, S. (2011). Not all brains are made the same: new views on brain scaling in evolution. *Brain Behav. Evol.* 78, 22–36.
7. Tosches, M.A. (2021). From Cell Types to an Integrated Understanding of Brain Evolution: The Case of the Cerebral Cortex. *Annu. Rev. Cell Dev. Biol.* 37, 495–517.
8. Kautt, A.F., Chen, J., Lewarch, C.L., Hu, C., Turner, K., Lassance, J.M., Baier, F., Bedford, N.L., Bendesky, A., and Hoekstra, H.E. (2024). Evolution of gene expression across brain regions in behaviourally divergent deer mice. *Mol. Ecol. Jan* 23, e17270.
9. Lee, D., Shahandeh, M.P., Abuin, L., and Benton, R. (2025). Comparative single-cell transcriptomic atlases of drosophilid brains suggest glial evolution during ecological adaptation. *PLoS Biol* 23, e3003120.
10. Oteiza, P., and Baldwin, M.W. (2021). Evolution of sensory systems. *Curr. Opin. Neurobiol.* 71, 52–59.
11. Ding, H., Smith, R.G., Poleg-Polsky, A., Diamond, J.S., and Briggman, K.L. (2016). Species-specific wiring for direction selectivity in the mammalian retina. *Nature* 535, 105–110.
12. Hong, R.L., Riebesell, M., Bumbarger, D.J., Cook, S.J., Carstensen, H.R., Sarpolaki, T., Cochella, L., Castrejon, J., Moreno, E., Sieriebriennikov, B., et al. (2019). Evolution of neuronal anatomy and circuitry in two highly divergent nematode species. *Elife* 8, e47155.
13. Bumbarger, D.J., Riebesell, M., Rödelberger, C., and Sommer, R.J. (2013). System-wide rewiring underlies behavioral differences in predatory and bacterial-feeding nematodes. *Cell* 152, 109–119.
14. Zhu, J., Boivin, J.C., Pang, S., Xu, C.S., Lu, Z., Saalfeld, S., Hess, H.F., and Ohyama, T. (2023). Comparative connectomics and escape behavior in larvae of closely related *Drosophila* species. *Curr. Biol.* 33, 2491–2503.
15. Schlegel, P., Bates, A.S., Stürmer, T., Jagannathan, S.R., Drummond, N., Hsu, J., Serratos Capdevila, L., Javier, A., Marin, E.C., Barth-Maron, A., et al. (2025). A single-cell transcriptomic atlas of *Drosophila* larval neurons reveals a conserved core of gene expression and a highly divergent set of cell-type-specific genes. *Nat. Neurosci.* 28, 105–117.

- A., et al. (2021). Information flow, cell types and stereotypy in a full olfactory connectome. *Elife* 10, e66018.
16. Bates, A.S., Schlegel, P., Roberts, R.J.V., Drummond, N., Tamimi, I.F.M., Turnbull, R., Zhao, X., Marin, E.C., Popovici, P.D., Dhawan, S., et al. (2020). Complete connectomic reconstruction of olfactory projection neurons in the fly brain. *Curr. Biol.* 30, 3183–3199.e6.
17. Fulton, K.A., Zimmerman, D., Samuel, A., Vogt, K., and Datta, S.R. (2024). Common principles for odour coding across vertebrates and invertebrates. *Nat. Rev. Neurosci.* 25, 453–472.
18. Jefferis, G.S., Marin, E.C., Stocker, R.F., and Luo, L. (2001). Target neuron prespecification in the olfactory map of *Drosophila*. *Nature* 414, 204–208.
19. Jefferis, G.S.X.E., Potter, C.J., Chan, A.M., Marin, E.C., Rohlfsing, T., Maurer, C.R., Jr., and Luo, L. (2007). Comprehensive maps of *Drosophila* higher olfactory centers: spatially segregated fruit and pheromone representation. *Cell* 128, 1187–1203.
20. Wong, A.M., Wang, J.W., and Axel, R. (2002). Spatial representation of the glomerular map in the *Drosophila* protocerebrum. *Cell* 109, 229–241.
21. Wong, K.K.L., Li, T., Fu, T.M., Liu, G., Lyu, C., Kohani, S., Xie, Q., Luginbuhl, D.J., Upadhyayula, S., Betzig, E., and Luo, L. (2023). Origin of wiring specificity in an olfactory map revealed by neuron type-specific, time-lapse imaging of dendrite targeting. *Elife* 12, e85521.
22. Li, T., Fu, T.M., Wong, K.K.L., Li, H., Xie, Q., Luginbuhl, D.J., Wagner, M.J., Betzig, E., and Luo, L. (2021). Cellular bases of olfactory circuit assembly revealed by systematic time-lapse imaging. *Cell* 184, 5107–5121.
23. Li, J., Han, S., Li, H., Udeshi, N.D., Svinkina, T., Mani, D.R., Xu, C., Guajardo, R., Xie, Q., Li, T., et al. (2020). Cell-surface proteomic profiling in the fly brain uncovers wiring regulators. *Cell* 180, 373–386.
24. Xie, Q., Brbic, M., Horns, F., Kolluru, S.S., Jones, R.C., Li, J., Reddy, A.R., Xie, A., Kohani, S., Li, Z., et al. (2021). Temporal evolution of single-cell transcriptomes of *Drosophila* olfactory projection neurons. *Elife* 10, e63450.
25. Knaden, M., Strutz, A., Ahsan, J., Sachse, S., and Hansson, B.S. (2012). Spatial representation of odorant valence in an insect brain. *Cell Rep.* 1, 392–399.
26. Strutz, A., Soelter, J., Baschwitz, A., Farhan, A., Grabe, V., Rybak, J., Knaden, M., Schmuker, M., Hansson, B.S., and Sachse, S. (2014). Decoding odor quality and intensity in the *Drosophila* brain. *Elife* 3, e04147.
27. Frechter, S., Bates, A.S., Tootoonian, S., Dolan, M.J., Manton, J., Jamasb, A.R., Kohl, J., Bock, D., and Jefferis, G. (2019). Functional and anatomical specificity in a higher olfactory centre. *Elife* 8, e44590.
28. Jeanne, J.M., Fisek, M., and Wilson, R.I. (2018). The organization of projections from olfactory glomeruli onto higher-order neurons. *Neuron* 98, 1198–1213.
29. Auer, T.O., Khallaf, M.A., Silbering, A.F., Zappia, G., Ellis, K., Álvarez-Ocaña, R., Arguello, J.R., Hansson, B.S., Jefferis, G.S.X.E., Caron, S.J.C., et al. (2020). Olfactory receptor and circuit evolution promote host specialization. *Nature* 579, 402–408.
30. Prieto-Godino, L.L., Rytz, R., Bargeton, B., Abuin, L., Arguello, J.R., Peraro, M.D., and Benton, R. (2016). Olfactory receptor pseudo-pseudogenes. *Nature* 539, 93–97.
31. Prieto-Godino, L.L., Rytz, R., Cruchet, S., Bargeton, B., Abuin, L., Silbering, A.F., Ruta, V., Dal Peraro, M., and Benton, R. (2017). Evolution of acid-sensing olfactory circuits in *Drosophilids*. *Neuron* 93, 661–676.
32. Prieto-Godino, L.L., Schmidt, H.R., and Benton, R. (2021). Molecular reconstruction of recurrent evolutionary switching in olfactory receptor specificity. *Elife* 10, e69732.
33. Dekker, T., Ibba, I., Siju, K.P., Stensmyr, M.C., and Hansson, B.S. (2006). Olfactory shifts parallel superspecialism for toxic fruit in *Drosophila melanogaster* sibling, *D. sechellia*. *Curr. Biol.* 16, 101–109.
34. Takagi, S., Sancer, G., Abuin, L., Stupski, S.D., Roman Arguello, J., Prieto-Godino, L.L., Stern, D.L., Cruchet, S., Álvarez-Ocaña, R., Wienecke, C.F.R., et al. (2024). Olfactory sensory neuron population expansions influence projection neuron adaptation and enhance odour tracking. *Nat. Commun.* 15, 7041.
35. Ellis, K.E., Bervoets, S., Smihula, H., Ganguly, I., Vigato, E., Auer, T.O., Benton, R., Litwin-Kumar, A., and Caron, S.J.C. (2024). Evolution of connectivity architecture in the *Drosophila* mushroom body. *Nat. Comm.* 15, 4872.
36. Combs, P.A., Krupp, J.J., Khosla, N.M., Bua, D., Petrov, D.A., Levine, J.D., and Fraser, H.B. (2018). Tissue-specific cis-regulatory divergence implicates *eloF* in inhibiting interspecies mating in *Drosophila*. *Curr. Biol.* 28, 3969–3975.
37. Holtzman, S., Miller, D., Eisman, R., Kuwayama, H., Niimi, T., and Kaufman, T. (2010). Transgenic tools for members of the genus *Drosophila* with sequenced genomes. *Fly (Austin)* 4, 349–362.
38. Groth, A.C., Fish, M., Nusse, R., and Calos, M.P. (2004). Construction of transgenic *Drosophila* by using the site-specific integrase from phage ϕ C31. *Genetics* 166, 1775–1782.
39. Bischof, J., Maeda, R.K., Hediger, M., Karch, F., and Basler, K. (2007). An optimized transgenesis system for *Drosophila* using germ-line-specific ϕ C31 integrases. *Proc. Natl. Acad. Sci. USA* 104, 3312–3317.
40. Meissner, G.W., Nern, A., Dorman, Z., DePasquale, G.M., Forster, K., Gibney, T., Hausenfluck, J.H., He, Y., Iyer, N.A., Jeter, J., et al. (2023). A searchable image resource of *Drosophila* GAL4 driver expression patterns with single neuron resolution. *Elife* 12, e80660.
41. Dionne, H., Hibbard, K.L., Cavallaro, A., Kao, J.C., and Rubin, G.M. (2018). Genetic reagents for making split-Gal4 lines in *Drosophila*. *Genetics* 209, 31–35.
42. Pfeiffer, B.D., Ngo, T.T.B., Hibbard, K.L., Murphy, C., Jenett, A., Truman, J.W., and Rubin, G.M. (2010). Refinement of tools for targeted gene expression in *Drosophila*. *Genetics* 186, 735–755.
43. Cachero, S., Ostrovsky, A.D., Yu, J.Y., Dickson, B.J., and Jefferis, G.S.X.E. (2010). Sexual dimorphism in the fly brain. *Curr. Biol.* 20, 1589–1601.
44. Manton, J.D., Ostrovsky, A.D., Goetz, L., Costa, M., Rohlfsing, T., and Jefferis, G.S. (2014). Combining genome-scale *Drosophila* 3D neuroanatomical data by bridging template brains. Preprint at bioRxiv, 006353. <https://doi.org/10.1101/006353>.
45. Peng, H., Chung, P., Long, F., Qu, L., Jenett, A., Seeds, A.M., Myers, E.W., and Simpson, J.H. (2011). BrainAligner: 3D registration atlases of *Drosophila* brains. *Nat. Methods* 8, 493–500.
46. Knapp, J.M., Chung, P., and Simpson, J.H. (2015). Generating customized transgene landing sites and multi-transgene arrays in *Drosophila* using ϕ C31 integrase. *Genetics* 199, 919–934.
47. Markstein, M., Pitsouli, C., Villalta, C., Celniker, S.E., and Perrimon, N. (2008). Exploiting position effects and the gypsy retrovirus insulator to engineer precisely expressed transgenes. *Nat. Genet.* 40, 476–483.
48. Jenett, A., Rubin, G.M., Ngo, T.T.B., Shepherd, D., Murphy, C., Dionne, H., Pfeiffer, B.D., Cavallaro, A., Hall, D., Jeter, J., et al. (2012). A GAL4-driver line resource for *Drosophila* neurobiology. *Cell Rep.* 2, 991–1001.
49. Stern, D.L., Stern, D.L., Crocker, J., Ding, Y., Frankel, N., Kappes, G., Kim, E., Kuzmickas, R., Lemire, A., Mast, J.D., and Picard, S. (2017). Genetic and transgenic reagents for *Drosophila simulans*, *D. mauritiana*, *D. yakuba*, *D. santomea*, and *D. virilis*. G3 (Bethesda). *Genetics* 7, 1339–1347.
50. Pfeiffer, B.D., Jenett, A., Hammonds, A.S., Ngo, T.T.B., Misra, S., Murphy, C., Scully, A., Carlson, J.W., Wan, K.H., Lavery, T.R., et al. (2008). Tools for neuroanatomy and neurogenetics in *Drosophila*. *Proc. Natl. Acad. Sci. USA* 105, 9715–9720.
51. Ibba, I., Angioy, A.M., Hansson, B.S., and Dekker, T. (2010). Macrogglomeruli for fruit odors change blend preference in *Drosophila*. *Naturwissenschaften* 97, 1059–1066.
52. Luan, H., Peabody, N.C., Vinson, C.R., and White, B.H. (2006). Refined spatial manipulation of neuronal function by combinatorial restriction of transgene expression. *Neuron* 52, 425–436.
53. Mellert, D.J., and Truman, J.W. (2012). Transvection is common throughout the *Drosophila* genome. *Genetics* 191, 1129–1141.

54. Shuai, Y., Sammons, M., Sterne, G.R., Hibbard, K.L., Yang, H., Yang, C.P., Managan, C., Siwanowicz, I., Lee, T., Rubin, G.M., et al. (2025). Driver lines for studying associative learning in *Drosophila*. *Elife* 13, RP94168.
55. Nern, A., Pfeiffer, B.D., and Rubin, G.M. (2015). Optimized tools for multi-color stochastic labeling reveal diverse stereotyped cell arrangements in the fly visual system. *Proc. Natl. Acad. Sci. USA* 112, E2967–E2976.
56. Jefferis, G.S.X.E., Vyas, R.M., Berdnik, D., Ramaekers, A., Stocker, R.F., Tanaka, N.K., Ito, K., and Luo, L. (2004). Developmental origin of wiring specificity in the olfactory system of *Drosophila*. *Development* 131, 117–130.
57. Court, R., Costa, M., Pilgrim, C., Millburn, G., Holmes, A., McLachlan, A., Larkin, A., Matentzoglou, N., Kir, H., Parkinson, H., et al. (2023). Virtual Fly Brain—An interactive atlas of the *Drosophila* nervous system. *Front. Physiol.* 14, 1076533.
58. Nern, A., Pfeiffer, B.D., Svoboda, K., and Rubin, G.M. (2011). Multiple new site-specific recombinases for use in manipulating animal genomes. *Proc. Natl. Acad. Sci. USA* 108, 14198–14203.
59. Costa, M., Manton, J.D., Ostrovsky, A.D., Prohaska, S., and Jefferis, G.S.X.E. (2016). NBLAST: Rapid, sensitive comparison of neuronal structure and construction of neuron family databases. *Neuron* 91, 293–311.
60. Depetris-Chauvin, A., Galagovsky, D., Keese, I.W., Hansson, B.S., Sachse, S., and Knaden, M. (2023). Evolution at multiple processing levels underlies odor-guided behavior in the genus *Drosophila*. *Curr. Biol.* 33, 4771–4785.e7.
61. Álvarez-Ocaña, R., Shahandeh, M.P., Ray, V., Auer, T.O., Gompel, N., and Benton, R. (2023). Odor-gated oviposition behavior in an ecological specialist. *Nat. Commun.* 14, 3041.
62. Dolan, M.J., Frechter, S., Bates, A.S., Dan, C., Huoviala, P., Roberts, R.J., Schlegel, P., Dhawan, S., Tabano, R., Dionne, H., et al. (2019). Neurogenetic dissection of the *Drosophila* lateral horn reveals major outputs, diverse behavioural functions, and interactions with the mushroom body. *Elife* 8, e43079.
63. Seeholzer, L.F., Seppo, M., Stern, D.L., and Ruta, V. (2018). Evolution of a central neural circuit underlies *Drosophila* mate preferences. *Nature* 559, 564–569.
64. Fouquet, W., Oswald, D., Wichmann, C., Mertel, S., Depner, H., Dyba, M., Hallermann, S., Kittel, R.J., Eimer, S., and Sigrist, S.J. (2009). Maturation of active zone assembly by *Drosophila* bruchpilot. *J. Cell Biol.* 186, 129–145.
65. Tobin, W.F., Wilson, R.I., and Lee, W.C.A. (2017). Wiring variations that enable and constrain neural computation in a sensory microcircuit. *Elife* 6, e24838.
66. Komiyama, T., Johnson, W.A., Luo, L., and Jefferis, G.S.X.E. (2003). From lineage to wiring specificity. POU domain transcription factors control precise connections of *Drosophila* olfactory projection neurons. *Cell* 112, 157–167.
67. Ding, Y., Berrocal, A., Morita, T., Longden, K.D., and Stern, D.L. (2016). Natural courtship song variation caused by an intronic retroelement in an ion channel gene. *Nature* 536, 329–332.
68. Ding, Y., Lillis, J.L., Cande, J., Berman, G.J., Arthur, B.J., Long, X., Xu, M., Dickson, B.J., and Stern, D.L. (2019). Neural evolution of context-dependent fly song. *Curr. Biol.* 29, 1089–1099.
69. Sato, K., and Yamamoto, D. (2023). Molecular and cellular origins of behavioral sex differences: a tiny little fly tells a lot. *Front. Mol. Neurosci.* 16, 1284367.
70. Tanaka, R., Higuchi, T., Kohatsu, S., Sato, K., and Yamamoto, D. (2017). Optogenetic activation of the *fruitless*-labeled circuitry in *Drosophila subobscura* males induces mating motor acts. *J. Neurosci.* 37, 11662–11674.
71. Ye, D., Walsh, J.T., Junker, I.P., and Ding, Y. (2024). Changes in the cellular makeup of motor patterning circuits drive courtship song evolution in *Drosophila*. *Curr. Biol.* 34, 2319–2329.
72. Coleman, R.T., Morante, I., Koreman, G.T., Cheng, M.L., Ding, Y., and Ruta, V. (2024). A modular circuit coordinates the diversification of courtship strategies. *Nature* 635, 142–150.
73. Reisenman, C.E., Wong, J., Vedagarbha, N., Lively, C., and Scott, K. (2023). Taste adaptations associated with host specialization in the specialist *Drosophila sechellia*. *J. Exp. Biol.* 226, jeb244641.
74. Abe, M., Kamiyama, T., Izumi, Y., Qian, Q., Yoshihashi, Y., Degawa, Y., Watanabe, K., Hattori, Y., Uemura, T., and Niwa, R. (2022). Shortened lifespan induced by a high-glucose diet is associated with intestinal immune dysfunction in *Drosophila sechellia*. *J. Exp. Biol.* 225, jeb244423.
75. Watanabe, K., Kanaoka, Y., Mizutani, S., Uchiyama, H., Yajima, S., Watanabe, M., Uemura, T., and Hattori, Y. (2019). Interspecies comparative analyses reveal distinct carbohydrate-responsive systems among *Drosophila* species. *Cell Rep.* 28, 2594–2607.
76. Melvin, R.G., Lamichane, N., Havula, E., Kokki, K., Soeder, C., Jones, C.D., and Hietakangas, V. (2018). Natural variation in sugar tolerance associates with changes in signaling and mitochondrial ribosome biogenesis. *Elife* 7, e40841.
77. Ding, S.D., Leitão, A.B., Day, J.P., Arunkumar, R., Phillips, M., Zhou, S.O., and Jiggins, F.M. (2022). Trans-regulatory changes underpin the evolution of the *Drosophila* immune response. *PLoS Genet.* 18, e1010453.
78. Joyce, M., Falconio, F.A., Blackhurst, L., Prieto-Godino, L., French, A.S., and Gilestro, G.F. (2024). Divergent evolution of sleep in *Drosophila* species. *Nat. Commun.* 15, 5091.
79. Shahandeh, M.P., Abuin, L., Lescuyer De Decker, L., Cergneux, J., Koch, R., Nagoshi, E., and Benton, R. (2024). Circadian plasticity evolves through regulatory changes in a neuropeptide gene. *Nature* 635, 951–959.
80. York, R.A., Brezovec, L.E., Coughlan, J., Herbst, S., Krieger, A., Lee, S.Y., Pratt, B., Smart, A.D., Song, E., Suvorov, A., et al. (2022). The evolutionary trajectory of *Drosophila* walking. *Curr. Biol.* 32, 3005–3015.
81. Tirian, L., and Dickson, B.J. (2017). The VT GAL4, LexA, and split-GAL4 driver line collections for targeted expression in the *Drosophila* nervous system. Preprint at bioRxiv, 198648. <https://doi.org/10.1101/198648>.
82. Lee, T., and Luo, L. (1999). Mosaic analysis with a repressible cell marker for studies of gene function in neuronal morphogenesis. *Neuron* 22, 451–461.
83. Arnould, L., Su, K.F.Y., Manoel, D., Minervino, C., Magriña, J., Gompel, N., and Prud'homme, B. (2013). Emergence and diversification of fly pigmentation through evolution of a gene regulatory module. *Science* 339, 1423–1426.
84. Gratz, S.J., Ukken, F.P., Rubinstein, C.D., Thiede, G., Donohue, L.K., Cummings, A.M., and O'Connor-Giles, K.M. (2014). Highly specific and efficient CRISPR/Cas9-catalyzed homology-directed repair in *Drosophila*. *Genetics* 196, 961–971.
85. Stern, D.L. (2022). Transgenic tools for targeted chromosome rearrangements allow construction of balancer chromosomes in non-melanogaster *Drosophila* species. *G3 (Bethesda)* 12, jkac030.
86. Chen, T.W., Wardill, T.J., Sun, Y., Pulver, S.R., Renninger, S.L., Baohan, A., Schreiter, E.R., Kerr, R.A., Orger, M.B., Jayaraman, V., et al. (2013). Ultrasensitive fluorescent proteins for imaging neuronal activity. *Nature* 499, 295–300.
87. Schindelin, J., Arganda-Carreras, I., Frise, E., Kaynig, V., Longair, M., Pietzsch, T., Preibisch, S., Rueden, C., Saalfeld, S., Schmid, B., et al. (2012). Fiji: an open-source platform for biological-image analysis. *Nat. Methods* 9, 676–682.
88. Feng, L., Zhao, T., and Kim, J. (2015). neuTube 1.0: A new design for efficient neuron reconstruction software based on the swc format. *eNeuro* 2, ENEURO.0049-14.2014.
89. Bates, A.S., Manton, J.D., Jagannathan, S.R., Costa, M., Schlegel, P., Rohlfing, T., and Jefferis, G.S. (2020). The natverse, a versatile toolbox for combining and analysing neuroanatomical data. *Elife* 9, e53350.
90. Plaza, S.M., Clements, J., Dolafi, T., Umayam, L., Neubarth, N.N., Scheffer, L.K., and Berg, S. (2022). neuPrint: An open access tool for EM connectomics. *Front. Neuroinform.* 16, 896292.
91. Chakraborty, M., Chang, C.H., Khost, D.E., Vedanayagam, J., Adrion, J.R., Liao, Y., Montooth, K.L., Meiklejohn, C.D., Larracuente, A.M., and

- Emerson, J.J. (2021). Evolution of genome structure in the *Drosophila simulans* species complex. *Genome Res.* **31**, 380–396.
92. Stern, D.L. (2017). Tagmentation-Based Mapping (TagMap) of mobile DNA genomic insertion sites. Preprint at bioRxiv, 037762. <https://doi.org/10.1101/037762>.
 93. Gohl, D.M., Silles, M.A., Gao, X.J., Bhalerao, S., Luongo, F.J., Lin, C.C., Potter, C.J., and Clandinin, T.R. (2011). A versatile *in vivo* system for directed dissection of gene expression patterns. *Nat. Methods* **8**, 231–237.
 94. Han, C., Jan, L.Y., and Jan, Y.N. (2011). Enhancer-driven membrane markers for analysis of nonautonomous mechanisms reveal neuron-glia interactions in *Drosophila*. *Proc. Natl. Acad. Sci. USA* **108**, 9673–9678.
 95. Port, F., Chen, H.M., Lee, T., and Bullock, S.L. (2014). Optimized CRISPR/Cas tools for efficient germline and somatic genome engineering in *Drosophila*. *Proc. Natl. Acad. Sci. USA* **111**, E2967–E2976.
 96. Port, F., and Bullock, S.L. (2016). Augmenting CRISPR applications in *Drosophila* with tRNA-flanked sgRNAs. *Nat. Methods* **13**, 852–854.
 97. Sanchez-Alcaniz, J.A., Zappia, G., Marion-Poll, F., and Benton, R. (2017). A mechanosensory receptor required for food texture detection in *Drosophila*. *Nat. Commun.* **8**, 14192.
 98. Arshadi, C., Günther, U., Eddison, M., Harrington, K.I.S., and Ferreira, T.A. (2021). SNT: a unifying toolbox for quantification of neuronal anatomy. *Nat. Methods* **18**, 374–377.

STAR★METHODS

KEY RESOURCES TABLE

REAGENT or RESOURCE	SOURCE	IDENTIFIER
Antibodies		
mouse monoclonal antibody nc82	Developmental Studies Hybridoma Bank	DSHB Cat Nr. nc82; RRID:AB_2314866
rat anti-Cadherin	Developmental Studies Hybridoma Bank	DSHB Cat Nr. MNCD2; RRID:AB_528119
anti-HA	Roche	Roche Cat Nr. 11867431001; RRID: AB_390919
anti-FLAG	Novus Biologicals	NB600-345
anti-GFP	Invitrogen	#A-11122
Cy3-goat anti-mouse	Molecular Probes, Jackson ImmunoResearch	115-165-003
Cy5-goat anti-rat	Molecular Probes, Jackson ImmunoResearch	112-175-143
Alexa 488-goat anti-rabbit	Molecular Probes, Jackson ImmunoResearch	111-545-003
Chemicals, peptides, and recombinant proteins		
Noni juice	Raab Vitalfood	RV-5766
methyl hexanoate	Sigma Aldrich	CAS 106-70-7
2-heptanone	Sigma Aldrich	CAS 110-43-0
dichloromethane	Sigma Aldrich	CAS 75-09-2
Deposited data		
<i>D. sechellia</i> PN traces and analysis code	Github/Zenodo	Github: https://github.com/AuerTomLab/Duerr2025 Zenodo: https://doi.org/10.5281/zenodo.15012945
<i>D. sechellia</i> raw imaging data etc.	Zenodo	Zenodo: https://doi.org/10.5281/zenodo.15002759
Experimental models: Drosophila strains		
<i>Dsec.07 (wildtype)</i>	<i>Drosophila</i> Species Stock Center [DSSC] 14021-0248.07	N/A
<i>Dsec.30 (white mutant)</i>	DSSC 14021-0248.30	N/A
<i>Dsec-attPpBac-A26</i>	piggyBac integration, this study	N/A
<i>Dsec-attP40</i>	CRISPR knock-in, this study	N/A
<i>Dsec-attP2</i>	CRISPR knock-in, this study	N/A
<i>Dsec-attPwhite</i>	Auer et al. ²⁹	N/A
<i>Dsec-attP1029</i>	CRISPR knock-in, this study	N/A
<i>Dsec-attPJK22C</i>	CRISPR knock-in, this study	N/A
<i>Dsec-su(Hw)attP2</i>	CRISPR knock-in, this study	N/A
<i>Dmel-GMR86C10-Gal4</i>	Bloomington <i>Drosophila</i> Stock Center [BDSC] 46820	N/A
<i>Dmel-VT033006-Gal4</i>	BDSC_73333	Tirian et al. ⁸¹
<i>Dsec-GMR86C10-Gal4@Dsec-attP40</i>	Takagi et al. ³⁴	N/A
<i>Dsec-GMR86C10-Gal4@Dsec-attP1029</i>	attB/P integration, this study	N/A
<i>Dsec-VT033006-Gal4</i>	Takagi et al. ³⁴	N/A
<i>Dsec-VT033008-Gal4</i>	Takagi et al. ³⁴	N/A
<i>Dmel-SS0186F</i>	Xie et al. ²⁴	SS0186F Split Gal4 line
<i>Dsec-VT033006 pGal4BD@white</i>	attB/P integration, this study	N/A
<i>Dsec-GMR72C11-p65AD@white</i>	attB/P integration, this study	N/A
<i>Dsec-GMR72C11-p65AD@Dsec-attPA26</i>		N/A
<i>Dmel-SS00587</i>	Shuai et al. ⁵⁴	SS00587 Split Gal4 line
<i>Dsec-GMR55A03- pGal4DB@Dsec-attPA26</i>	attB/P integration, this study	N/A

(Continued on next page)

Continued

REAGENT or RESOURCE	SOURCE	IDENTIFIER
<i>Dsec-GMR50E01-p65AD@white</i>	attB/P integration, this study	N/A
<i>Dsim-VT033006Gal4</i>	attB/P integration, this study	N/A
<i>Dsim-Nsyb-Gal4</i>	Ellis et al. ³⁵	N/A
<i>Dsec-20xUAS-GCaMP6s</i>	attB/P integration, this study	N/A
<i>Dsec-UAS-CD4:GFP</i>	CRISPR knock-in, this study	N/A
<i>Dsec-UAS-C3PA-GFP</i>	Auer et al. ²⁹	N/A
<i>Dsec-UAS-Brp-short^{mStraw}</i>	P element integration, this study	N/A
<i>Dsec-UAS-GCaMP6f</i>	Auer et al. ²⁹	N/A
<i>Dmel-5xUAS-mCD8:GFP</i>	Lee et al. ⁸²	N/A
<i>Dmel-20xUAS-GFP</i>	BDSC_52262	N/A
<i>Dmel-20xUAS-GCaMP6s</i>	BDSC_42746	N/A
<i>Dsim-UAS-GCaMP6s</i>	Seeholzer et al. ⁶³	N/A
<i>Dsim-UAS-C3PA-GFP</i>	Ellis et al. ³⁵	N/A
<i>Dsec-flp-out@Dsec-attP40</i>	CRISPR knock-in, this study	N/A
<i>Dsec-flp-out@Dsec-attP1029</i>	CRISPR knock-in, this study	N/A
<i>Dsec-hs-Flp1</i>	attB/P integration, this study	N/A
<i>Dmel-MCF0-1</i>	BDSC_64085	N/A
Oligonucleotides		
Primers to generate single sgRNA plasmids, see Table S6		N/A
Primers to generate multiple sgRNA plasmids, see Table S7		N/A
Recombinant DNA		
pBS130	Addgene	26290
<i>piggyBac</i> helper plasmid	Arnoult et al. ⁸³	N/A
<i>P element</i> helper plasmid	Stern et al. ⁴⁹	N/A
<i>pBac(attP-3P3-YFP)</i>	Addgene	86860
<i>pHD-DsRed-attP</i>	Gratz et al. ⁸⁴	N/A
<i>pUC57-MHC-DsRed</i>	Stern et al. ⁸⁵	N/A
<i>p3xP3-YFP-attP</i>	Stern et al. ⁴⁹	N/A
<i>pJFRC208-10XUAS-FRT>STOP>FRT-myr::smGFP-FLAG</i>	Addgene	63169
<i>pJFRC208-10XUAS-FRT>STOP>FRT-myr::smGFP-HA</i>	Addgene	63166
<i>pCFD3-dU6-3gRNA</i>	Addgene	49410
<i>pCFD5</i>	Addgene	73914
<i>pUAS-Brp-short^{mStraw}</i>	Fouquet et al. ⁶⁴	N/A
<i>p(GP-JFRC7-20XUAS-IVS-GCaMP6s)</i>	Chen et al. ⁸⁶	N/A
<i>pVT033006-Gal4</i>	Tirian et al. ⁸¹	N/A
<i>pBPhsFlp1</i>	Addgene	32148
Software and algorithms		
Fiji	Schindelin et al. ⁸⁷	N/A
Amira 6.5	Thermo Fisher Scientific	N/A
neuTube 1.0z	Feng et al. ⁸⁸	N/A
natverse	Bates et al. ⁸⁹	N/A
neuprint	Plaza et al. ⁹⁰	N/A
R v3.2.3	R-project-org	N/A
Other		
<i>D. sechellia</i> ASM438219v2 genome assembly	Chakraborty et al. ⁹¹	N/A
TagMap	Stern et al. ⁹²	N/A

EXPERIMENTAL MODEL DETAILS

Drosophila husbandry

Drosophila stocks were maintained on standard wheat flour–yeast–fruit-juice medium under a 12-h light:12-h dark cycle at 25°C. For all *D. sechellia* strains, formula 4-24 instant *Drosophila* medium, blue (Carolina Biological Supply) soaked in noni juice (Raab Vitalfood) was added on top of the standard food. A detailed list of wildtype and transgenic lines used and generated in this study can be found in the key resource table. Sex and age of animals is listed in the respective method section.

METHOD DETAILS

Drosophila microinjections

Transgenesis of *D. sechellia* was performed in-house as described²⁹ (<http://gompel.org/methods>) with exception of *P-element* transgenesis performed by WellGenetics. In detail, *D. sechellia* flies were raised on standard food supplemented with noni juice-soaked formula 4-24 instant *Drosophila* medium prior to injections. Approximately 200 flies were transferred into mating cages and egg collection was performed on agar plates containing noni instead of grape juice and a supplement of noni juice-soaked instant medium on the surface. Embryos were manually selected for stage 2 prior to alignment and injection. For *piggyBac* and *P-element* transgenesis, a *piggyBac* or *P-element* vector (300 ng μL^{-1}) and *piggyBac*⁸³ or *P-element* helper plasmid⁴⁹ (300 ng μL^{-1}) were co-injected. For CRISPR–Cas9-mediated homologous recombination, a mix of a sgRNA-encoding construct (150 ng μL^{-1}) and donor vector (400 ng μL^{-1}) was injected into *Dsec nanos-Cas9*.²⁹ Site-directed integration into *attP* sites was achieved by co-injection of an *attB*-containing vector (400 ng μL^{-1}) and pBS130 (400 ng μL^{-1}) (encoding PhiC31 integrase under control of a heat shock promoter (Addgene #26290, ref. ⁹³), no heat shock was performed as basal expression was sufficient for transgenesis). All concentrations are given as final values in the injection mix. Insertion efficiencies for *attP* sites are listed in Table S2.

Molecular cloning

piggyBac-attP vector: We generated an *attP* site containing *piggyBac* vector marked with 3xP3-DsRed expression by replacing the 3xP3-YFP cassette in *pBac(attP-3P3-YFP)*⁴⁹ (Addgene #86860) with a floxed 3xP3-DsRed cassette from *pHD-DsRed-attP*⁸⁴ via Gibson Assembly.

Donor vectors for homologous recombination: Homology arms (0.8–1.6 kb) for individual target loci were amplified from *D. sechellia* (*Drosophila* Species Stock Center [DSSC] 14021–0248.07) genomic DNA and inserted into the respective donor vector backbone using either restriction cloning or Gibson Assembly. For *Dsec-attP2*, *Dsec-attPJK22C*, and *Dsec-attP40*, homology arms were inserted into *pHD-DsRed-attP*⁸⁴ via restriction cloning.

Dsec-su(Hw)attP2: We introduced an FRT site into *pHD-DsRed-attP* by adding its sequence to a PCR amplicon together with NcoI, BamHI overhangs and inserted the digested amplicon into the NcoI/BamHI digested *pHD-DsRed-attP* backbone resulting in *pHD-FRT-DsRed-attP*. Homology arms for the *su(Hw)attP2* locus were amplified from *D. sechellia* (DSSC 14021–0248.07) genomic DNA and inserted into *pHD-FRT-DsRed-attP* via restriction cloning.

Dsec-attP1029: We generated a *pHD-mhc-FRT-mFRT71-YFP* donor vector by amplification of three individual PCR amplicons from *pHD-DsRed-attP*, *pUC57-MHC-DsRed*⁸⁵ and *p3xP3-YFP-attP*.⁴⁹ PCR primers included overhangs generating the *FRT-mFRT71* sites and all three amplicons were combined to a single vector via Gibson assembly. Homology arms for the *Dsim1029* homologous locus⁴⁹ were amplified from *D. sechellia* (DSSC 14021–0248.07) genomic DNA and inserted via restriction cloning and Gibson Assembly resulting in *Dsec1029-mhc-YFP*.

UAS-CD4-GFP: To insert a *UAS-CD4-GFP* transgene at the *attP40* equivalent site of *D. sechellia*, we integrated a *UAS-CD4-GFP* cassette⁹⁴ into *Dsec-attP40-3xP3-DsRed* via Gibson assembly.

Flp-out constructs: We amplified the flp-out cassette from *pJFRC208-10XUAS-FRT>STOP>FRT-myr::smGFP-FLAG*⁵⁵ (Addgene #63169) via PCR and integrated it into *Dsec1029-mhc-YFP* via Gibson assembly resulting in *Dsec1029-flip-out-mhc-YFP*. Similarly, *DsecattP40-flip-out-3xP3-DsRed* was generated by PCR amplification of *pJFRC208-10XUAS-FRT>STOP>FRT-myr::smGFP-HA*⁵⁵ (Addgene #63166) and integration into *Dsec-attP40-3xP3-DsRed*.

Single guide RNA expression vectors: For expression of individual single guide (sg)RNAs, oligonucleotide pairs (Table S6) were annealed and cloned into BbsI-digested *pCFD3-dU6-3gRNA* (Addgene #49410), as previously described.⁹⁵ To express multiple sgRNAs from the same vector backbone, oligonucleotide pairs (Table S7) were used for PCR and inserted into *pCFD5* (Addgene #73914) via Gibson Assembly, as previously described.⁹⁶

Insertion site mapping

Mapping of *piggyBac* insertions using TagMap was performed as previously described.⁹² Sequencing hits were blasted against the *D. sechellia* ASM438219v2 genome assembly.⁹¹ Locations of transgene insertion sites are listed in Table S1.

Flp-out mediated stochastic labeling

For stochastic labeling, we combined *D. sechellia* Gal4 driver lines (*VT033006-Gal4*, *VT033008-Gal4* or *GMR86C10-Gal4*) with *Dsec-hs-Flp1* and crossed both transgenes to homozygosity. The resulting double-transgenic lines were crossed to homozygous

Dsec-attP1029-flip-out-mhc-YFP, *DsecattP40-flip-out-3xP3-DsRed* or flies homozygous for both resulting in experimental flies carrying one copy each of 3 or 4 of these transgenes. In *D. melanogaster*, we combined *D. melanogaster* Gal4 driver with MCF0-1.⁵⁵ The resulting F1 progeny was heat shocked for 3–5 min at 37°C in an incubator at the larval L3 stage, 24 h, 48 h, or 72 h after pupa formation. Heat shock length was determined in preliminary experiments aiming for stochastic labeling in few, ideally single neurons per brain hemisphere. Brains of emerging flies were dissected 5 days post-eclosion and stained with combinations of anti-GFP, anti-FLAG, anti-HA, anti-Cadherin and anti-nc82 antibodies as described in the immunohistochemistry section.

Immunohistochemistry

Immunofluorescent stainings on adult brains were performed as previously described⁹⁷ using mouse monoclonal antibody nc82 1:5, rat anti-Cadherin 1:25 (both Developmental Studies Hybridoma Bank), rat anti-HA 1:500 (Roche), rabbit anti-FLAG 1:500 (Novus Biologicals), and rabbit anti-GFP 1:500 (Invitrogen). Alexa 488-, Cy3- and Cy5-conjugated goat anti-mouse, goat anti-rat and goat anti-rabbit IgG secondary antibodies (Molecular Probes, Jackson ImmunoResearch) were used at 1:500.

Image acquisition and processing

Confocal images of brains were acquired on an inverted confocal microscope (Zeiss LSM 710) equipped with an oil immersion 40× objective (Plan Neofluar 40× oil immersion DIC objective; 1.3 NA), unless stated otherwise. For whole brain z-stacks, an x/y dimensions of 768 × 768px (354,25 × 354,25μm) was used and slice thickness was set to 1μm without slice overlap. The pinhole was set to 1AU (~2.17μm). The number of slices ranged between 170 and 190. Images were processed in Fiji.⁸⁷ *D. sechellia* brains were registered to the *D. sechellia* reference DsecF and subsequently to DsecI²⁹ and *D. melanogaster* brains to the IS2 *D. melanogaster* reference brain using the Fiji CMTK plugin (<https://github.com/jefferis/fiji-cmtk-gui>), as previously described.⁴³ The resulting registered brains were manually inspected and discarded if obvious deformations or registration artifacts were observed. All raw imaging data can be accessed at Zenodo (DOI: <https://doi.org/10.5281/zenodo.15002759>).

Antennal lobe segmentation & neuron reconstruction: Segmentation of the *D. sechellia* reference brain AL was performed on the nc82 signal using Amira 6.5 (Thermo Fisher Scientific) based on similar re-constructions.^{35,60} Projection neuron (PN) morphologies were manually traced using neuTube 1.0z.⁸⁸ PN identity was later assigned based on dendritic glomerular innervation in the AL, axonal branching pattern in the LH, and NBLAST clustering.

Comparison of neuron morphologies: Intra- and interspecific comparisons of *D. sechellia* and *D. melanogaster* PNs were performed using the R-based natverse ecosystem.⁸⁹ For the *D. melanogaster* datasets, we extracted neuron traces of adult AL PNs generated by light imaging and volumetric electron microscopy from the Virtual Fly Brain collection⁵⁷ (VFB ID: FBbt:00067123: “adult antennal lobe projection neuron”). Neurons were filtered to extract anterior dorsal (adPN) or lateral (IPN) PN types which were then bridged from JRC2018U over JRC2018F and FCWB to the IS2 reference space⁴³ (using natverse) and all left-hemisphere neurons were mirrored to the right hemisphere (see Figure S3A for a workflow overview). For some neurons, we detected erroneous annotations of cell somata and removed these somata from the visualization in Figure 3.

The *D. sechellia* dataset curation is described in detail in the R scripts deposited at GitHub (<https://github.com/AuerTomLab/Duerr2025>) and Zenodo (DOI: <https://doi.org/10.5281/zenodo.15012945>). Briefly, neurons traced in the unregistered *D. sechellia* brains were down scaled (by a dividing factor of 2.16796 on the x/y axis to translate pixels to μm) and individually registered to DsecF applying CMTK-based registrations of their corresponding brains. *D. sechellia* traces were bridged from DsecI to IS2 and all left-hemisphere neurons were mirrored to the right hemisphere. For intraspecific analysis, *D. sechellia* neurons were bridged to DsecI (traces are depicted in orthogonal view). To assess registration-introduced changes in brain morphology, Jacobian Determinant maps were generated using the CMTK command line tool and visualised using Fiji.

Neuron trace pruning: To compare neuron traces between *D. melanogaster* and *D. sechellia*, we used whole neuron traces and manually trimmed them in neuTube. In a first pruning step, we removed AL dendrite innervations; in a second step, we trimmed neuron traces up to a pre-defined vertical plane to only contain PN axonal traces including MB and LH branches.

Measurements of branch length: Branch length measurements were performed on traced neurites using the simple neurite tracer toolbox⁹⁸ (axons) or neuTube (dendrites). To quantify the branch length of the extra-branch in VM5d axons in *D. sechellia* and *D. melanogaster*, we took the branches from the branchpoint with the main PN axon to the most distal tip into account. To quantify the branch length in VM5d dendrites, we summed up the length of all dendritic branches outside the cognate VM5d glomerulus.

Connectomic circuit identification: Potential downstream neurons of *D. sechellia* PN innervations were identified in the *D. melanogaster* hemibrain (v1.2.1) by spatial proximity using neuprint⁹⁰. In detail, segmentation of previously annotated brain areas (LH, SLP, SCL) were downloaded from the Virtual Fly Brain, an axonal tract annotated in Amira, and plotted together with VM5d neurons in R (Figure S6A). An electron microscopy reconstruction of a *D. melanogaster* DM2 PN in close physical proximity to the *D. sechellia* VM5d extra branch area was selected in neuprint. Using this neuron as anchor point, horizontal and vertical EM sections relative to the DM2 branching direction (marked with white dotted lines in Figures S6B and S6C) were selected for visualization (additional details are listed in the accompanying R scripts). In these cross-sections, neurons were pseudo-coloured and labeled using Adobe Illustrator based on their annotations on neuprint (Figures S6B and S6C). These neurons were plotted in the IS2 brain space together with *D. sechellia* VM5d neurons using R.

***In vivo* two-photon calcium imaging and photoactivation**

Two-photon calcium imaging, odor delivery, image analysis and photoactivation was performed as described previously³⁴ with the exception that for odor delivery, the constant air flow in the olfactometer was not humidified. Noni juice (Raab Vitalfood) was diluted in water. Methyl hexanoate (CAS 106-70-7) and 2-heptanone (CAS 110-43-0) of the highest purity were purchased from Sigma Aldrich and diluted in dichloromethane (Sigma Aldrich, CAS 75-09-2).

QUANTIFICATION AND STATISTICAL ANALYSIS

Preliminary experiments were used to assess variance and determine adequate sample sizes in advance of acquisition of the reported data. Data were analyzed and plotted using Excel and R (v3.2.3; R Foundation for Statistical Computing, Vienna, Austria, 2005; R-project-org). Details about the statistical tests used are listed in the respective figure legend.

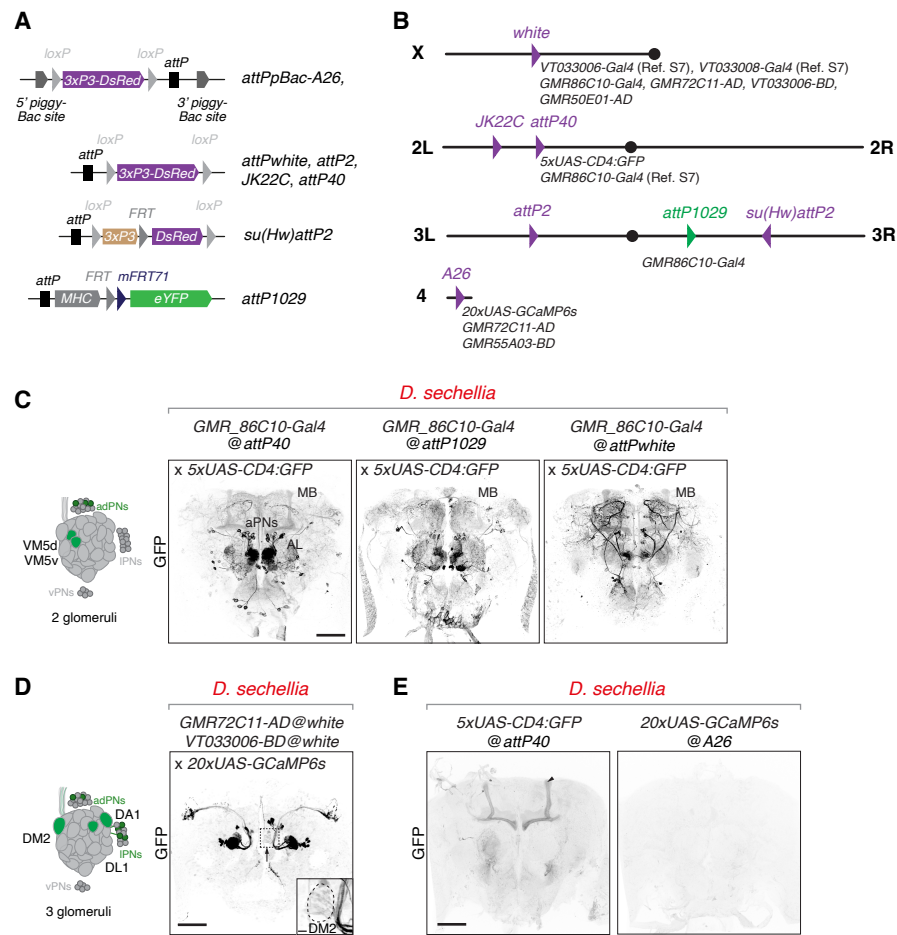
Cell Reports, Volume 44

Supplemental information

Olfactory projection neuron rewiring in the brain of an ecological specialist

Benedikt R. Dür, Enrico Bertolini, Suguru Takagi, Justine Pascual, Liliane Abuin, Giovanna Lucarelli, Richard Benton, and Thomas O. Auer

Supplementary Figure 1



Supplementary Figure 1. *attP* landing site establishment in *D. sechellia*.

A) Left: Schematic of the insertion cassettes used for piggyBac- and CRISPR-Cas9-mediated integration. The *FRT* and *mFRT71* sites placed between promoter and fluorescent marker do not interfere with expression. MHC = *myosin heavy chain* promoter (673bp version [S1]). Right: Integration sites established with these markers at random (piggyBac) and homologous locations to characterised sites in *D. melanogaster* (*attP2* [S2], *attP40* [S3], *JK22C* [S4], *su(Hw)attP2* [S5]) and *D. simulans* (insertion no.1029 [S6]).

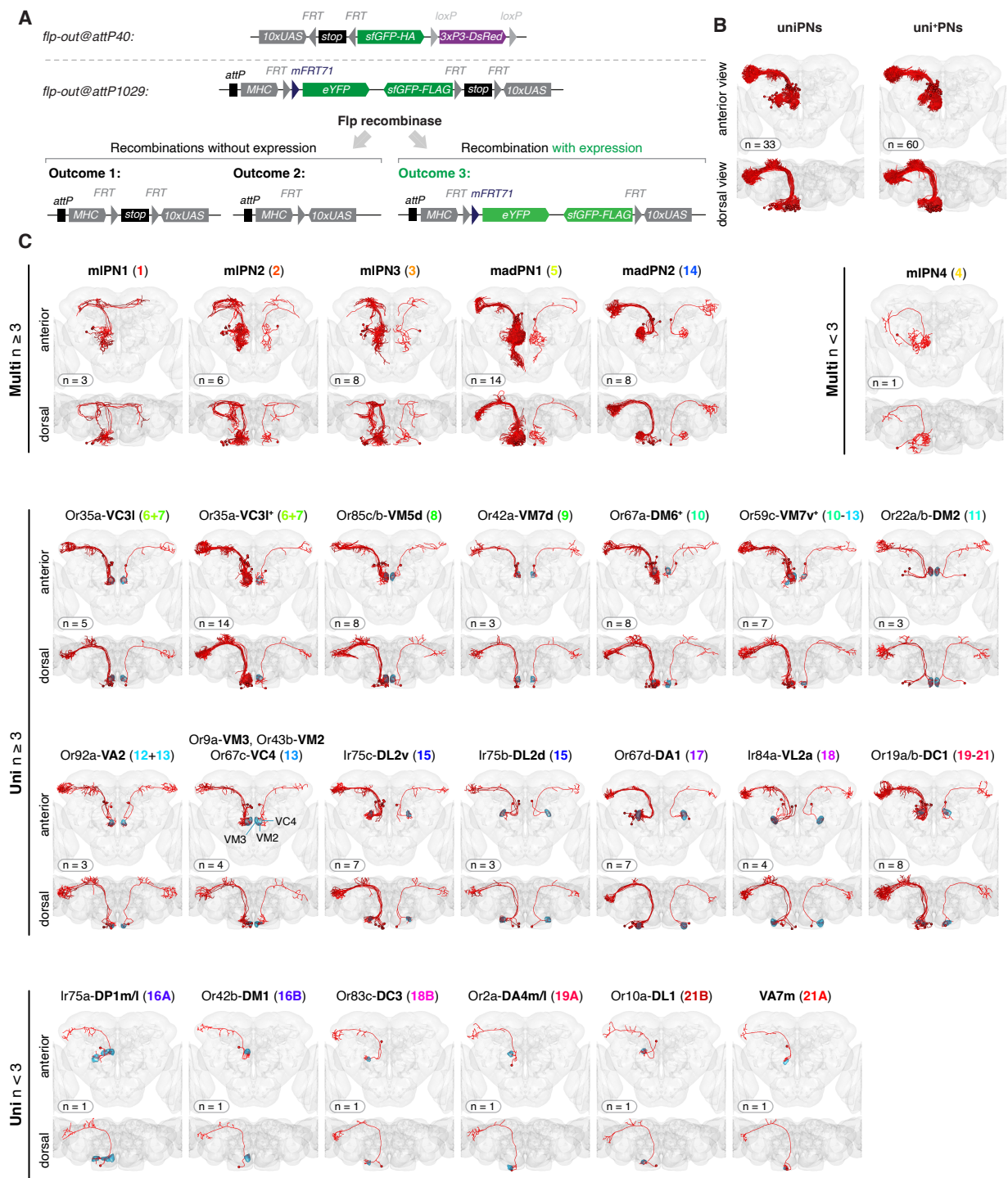
B) Location of *attP* sites on the four chromosomes of the *D. sechellia* genome. Black dot = centromere. Indicated below selected sites: transgenic constructs integrated via PhiC31-mediated transgenesis and used in panels **C-E** and **Figure 1**. Some transgenes have been published in Ref. [S7] as indicated.

C) Comparison of *GMR86C10-Gal4* driven expression from three different locations indicates positional effects of the respective *attP* site with increased background expression at the *white* locus (images for the other two locations same as **Figure 1C**).

D) Labeling of the DM2, DA1, and DL1 glomeruli by a split-Gal4 combination in *D. sechellia* combined with a *20xUAS-GCaMP6s* reporter. The 2-3 additional glomeruli shown in **Figure 1D** are not visible with this reporter – expression in DM2 (black arrow) is weak. Scale bar = 50 μ m. Insets: labeling of DM2. Scale bar = 5 μ m.

E) Anti-GFP immunofluorescence of the *D. sechellia* central brain of two *UAS*-reporter lines without Gal4 driver. The reporter integrated at the *Dsec-attP40* locus shows weak GFP expression in Kenyon cells (black arrows). Scale bar = 50 μ m.

Supplementary Figure 2



Supplementary Figure 2. Overview of *D. sechellia* PN cell types.

A) Top: schematics of the Flp-cassette at the *Dsec-attP40* locus. Below: schematics of the Flp-cassette at the *Dsec-attP1029* locus and potential outcomes of Flp recombinase-mediated recombination events. The *attP* landing site marker contains already a *FRT* site, resulting in multiple possible recombination events. Only outcome 3 leads to functional reporter expression (further increasing label sparseness with this transgene).

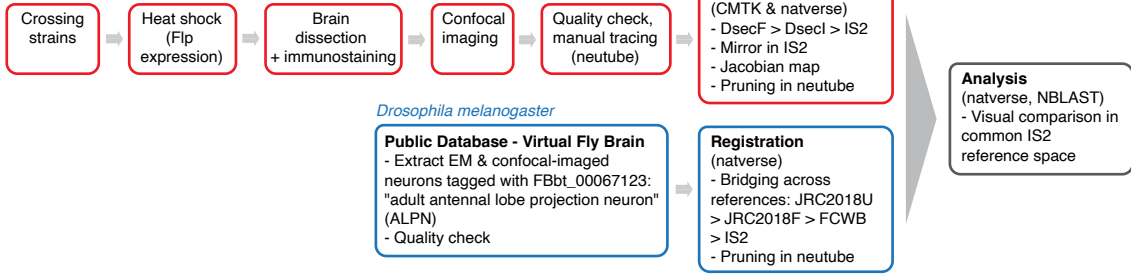
B) Classification of the 93 traced uPNs into 33 uniPNs and 60 uni⁺PNs.

C) Overview of the 26 PN types identified in the *D. sechellia* dataset. Left hemisphere: all neurons of the respective type; right hemisphere: individual representative neuron. Blue: segmentation of AL glomerulus/i with main dendritic innervation. Top row: 6 types of mPNs. 2 middle rows: uPNs with more than 3 examples in the dataset. Bottom row: uPNs with < 3 examples in the dataset.

Supplementary Figure 3











A

Drosophila sechellia



B

B

	Original Traces in DsecF	DsecF (warp)	DsecI (warp)	IS2 (affine + mirror)	IS2 (warp + mirror)
anterior					
dorsal					

C

C

Original Traces
in DsecF

DsecF
(warp)

DsecI
(warp)

IS2
(warp)

IS2
(warp + mirror)

anterior

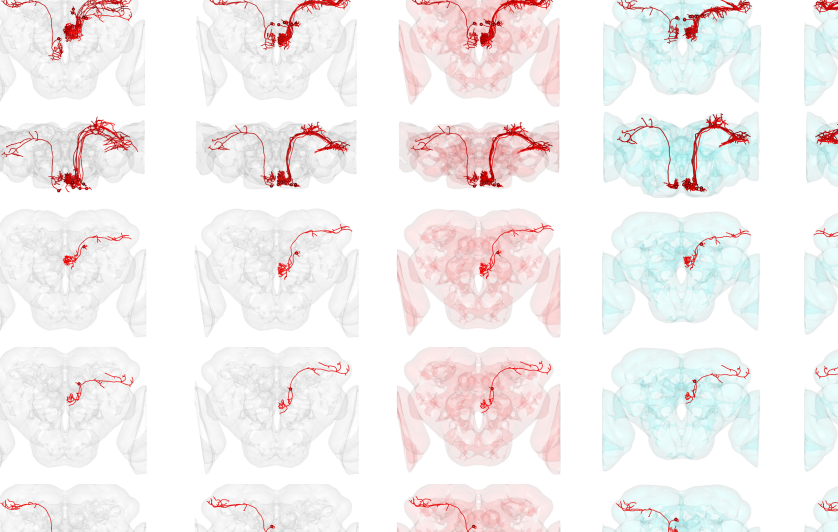
dorsal

All VM5d
PNs

neuron 1

neuron 2

neuron 3



D

[illegible]

Supplementary Figure 3. Comparison of *D. sechellia* and *D. melanogaster* brain templates.

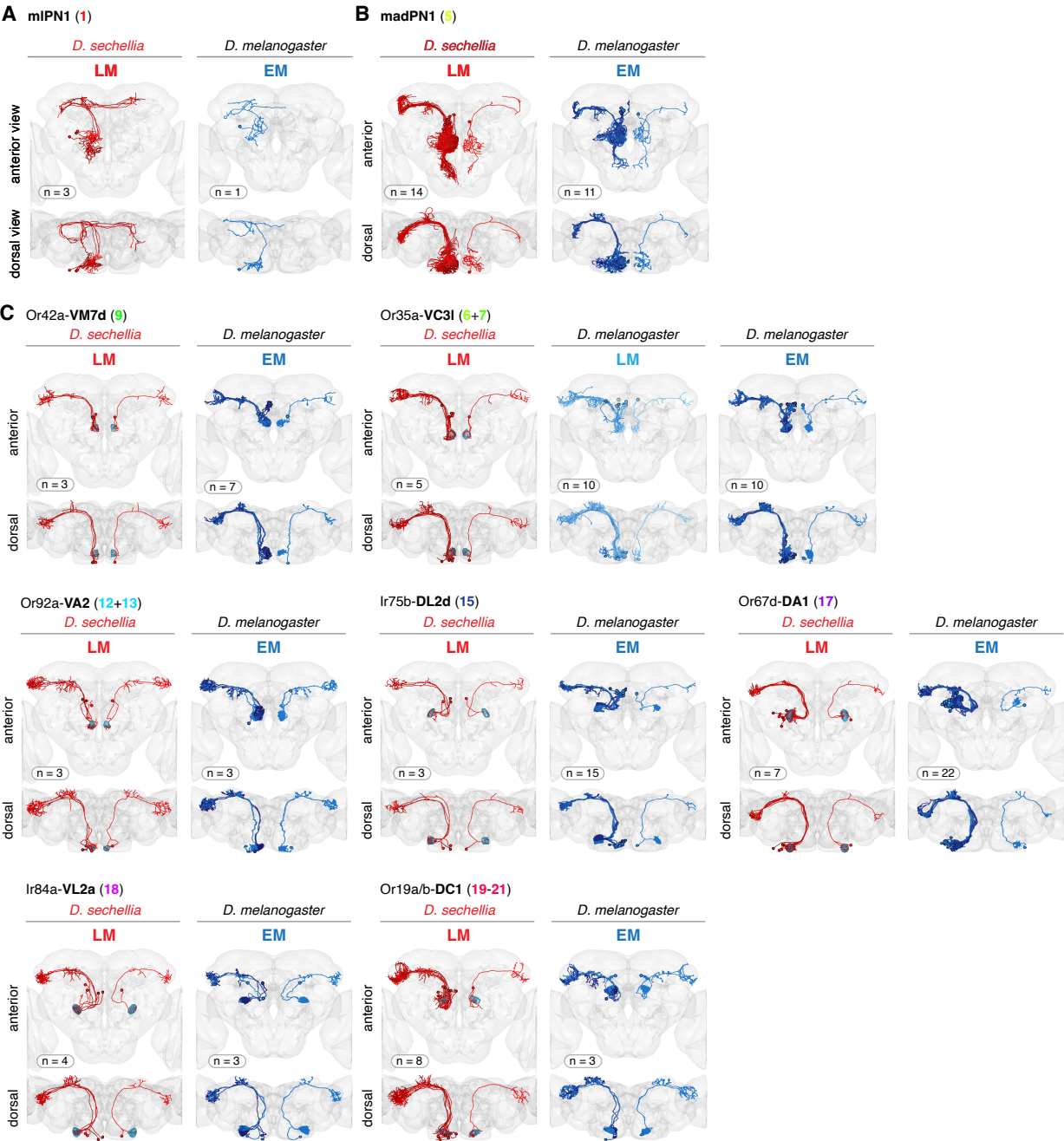
A) Summary of the workflow to generate and compare single neuron morphologies of *D. sechellia* with published *D. melanogaster* data.

B) Comparison of the original PN traces (red) in the DsecF (female) reference brain (left), after affine and warp registration in DsecF and DsecI (middle), and after affine and warp registration (and mirroring) in the *D. melanogaster* reference brain IS2 (right). Shown are 51 exemplary *D. melanogaster* PNs (in blue).

C) Visualization of all *D. sechellia* VM5d PNs (top) and three representative examples (below). Comparison of the original PN traces in the DsecF (female) reference brain (left), after affine and warp registration in DsecF and DsecI (middle), and after affine and warp registration (and mirroring) in the *D. melanogaster* reference brain IS2 (right).

D) NBLAST clustering using either whole neuron skeletons (left), neuron skeletons lacking AL dendritic innervations (middle) or MB and LH innervations only (right) for VM5d and DL2v PNs. Shown are also the respective neuron traces (*D. sechellia* light microscopy, LM, data in red, *D. melanogaster* LM data in light blue, electron microscopy, EM, data in dark blue).

Supplementary Figure 4



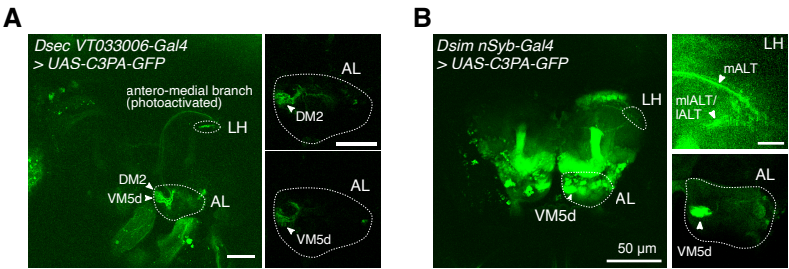
Supplementary Figure 4. Conserved PN morphologies between *D. melanogaster* and *D. sechellia*.

A) Comparison of mlPN1 morphologies between *D. sechellia* (left, light microscopy, LM) and *D. melanogaster* (right, electron microscopy, EM). Here, no individual examples are shown as axons of neurons with soma in the left hemisphere cross to the right hemisphere. The shorter contra-lateral branch in the *D. melanogaster* EM example could result from incomplete tracing across hemispheres.

B) Dorsal madPN1s in *D. sechellia* and *D. melanogaster*.

C) Comparison of seven uPN types between *D. sechellia* (left, LM) and *D. melanogaster* (right, LM and EM) with conserved neuroanatomy.

Supplementary Figure 5

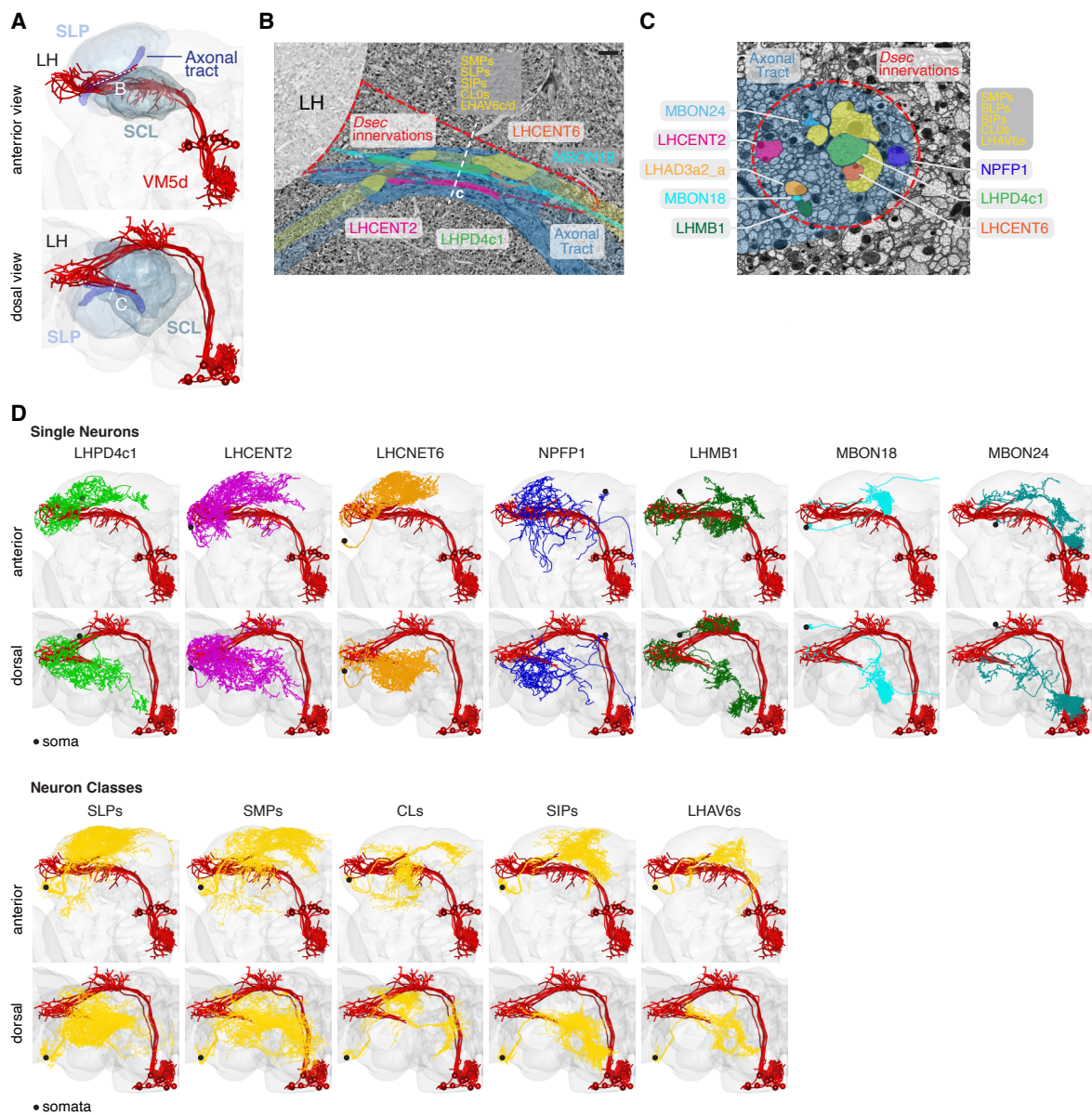


Supplementary Figure 5. Specific labeling of PN subtypes via photoactivation.

A) Photoactivation of the antero-medial branch area in *D. sechellia* expressing photo-activatable GFP in most PNs results in labeling of the DM2 and VM5d glomeruli. Left: Picture of the whole brain with labelling of the branch area and DM2 and VM5d innervating dendrites in the AL. Scale bar = 50 μ m. Right: higher magnification pictures of the AL showing DM2 (top) and VM5d (bottom) innervations. Scale bar = 25 μ m.

B) Photoactivation of VM5d innervating PNs in *D. simulans* expressing photo-activatable GFP pan-neuronally. Left: Picture of the whole brain with labelling of VM5d and projections to the LH. Scale bar = 50 μ m. Right, top: Higher magnification pictures of the LH. White arrowheads: medial AL tract (mALT), medial inhibitory AL tract (mIALT), and inhibitory AL tract (IALT). No branching into the antero-medial brain region is detected. Scale bar = 10 μ m. Bottom: Overview of the AL with only the VM5d glomerulus being labeled.

Supplementary Figure 6



Supplementary Figure 6. Potential *D. sechellia* VM5d/DM2 PN downstream partners based on connectomic data in *D. melanogaster*.

A) Same as **Fig. 4G**: relative location of the *D. sechellia* specific axonal PN branch between the superior lateral protocerebrum (SLP) and the superior clamp (SCL). White line anterior view: plane of cross-section panel **B**; white line dorsal view: plane of cross-section panel **C**.

B, C) EM section along (**B**) and perpendicular (**C**) to the axonal tract region. Red borders: novel PN innervations in *D. sechellia*. Blue: axonal tract. Several neurons (in colours) in *D. melanogaster* are in close proximity and potential downstream partners in *D. sechellia*. For a complete list of neurons in this target area, see **Table S5**.

D) 3D reconstruction of neurons indicated in **B, C** in *D. melanogaster* together with VM5d PNs of *D. sechellia* (red, in the IS2 reference space). Either individual neurons (top) or neuron classes (bottom) are shown. Black dots = neuron somata.

Table S1. Genomic locations of *piggyBac* insertions, related to Figure 1.
In blue = *attP* site used in this study.

Line	insertion site 1	insertion site 2	insertion site 3	Line identifier
<i>pBac(3xP3-DsRed-attP) line1</i>	4:153567..153646	2R:4811108..4811187		<i>pBac-attPA26</i>
<i>pBac(3xP3-DsRed-attP) line2</i>	2L:14348441..14348520	3R:16025079 ..16025158	3R:19267358..19267431	
<i>pBac(3xP3-DsRed-attP) line3</i>	2L:1671000..1671079			
<i>pBac(3xP3-DsRed-attP) line4</i>	3R:29972636..29972715	2R:13659569..13659634	2R:249042..248987 plus more hits in unplaced scaffold	
<i>pBac(3xP3-DsRed-attP) line5</i>	2L:164876..164955			
<i>pBac(3xP3-DsRed-attP) line6</i>	3R:11614682..11614757			
<i>pBac(3xP3-DsRed-attP) line7</i>	3R:5942576..5942655			
<i>pBac(3xP3-DsRed-attP) line8</i>	2L:8933864..8933943	2L:8511811..8511888		
<i>pBac(3xP3-DsRed-attP) line9</i>	2L:20760141..20760220	3L:3088544..3088623	2R:11531861..11531940	
<i>pBac(3xP3-DsRed-attP) line10</i>	2L:5476901..5476980			
<i>pBac(3xP3-DsRed-attP) line11</i>	2L:19742199..19753434			

Table S2. Efficiencies of transgene integration at *attP* sites, related to Figure 1.

<i>attP</i> site tested	Construct	No. embryos injected	No. fertile crosses	No. transgenic progeny	Efficiency (transgenic progeny/fertile crosses)
<i>Dsec-attP1029</i>	<i>GMR_86C10Gal4</i>	600	98	1	1%
<i>Dsec-attP40</i>		762	77	1	1.3%
<i>Dsec-attP2</i>		940	76	0	0
<i>Dsec-attPpBac-A26</i>		525	56	0	0
<i>Dsec-attPsu(Hw)attP2</i>		560	51	0	0
<i>Dsec-attPJK22C</i>		Homozygous lethal in <i>D. sechellia</i>			
<i>Dsec-attPwhite</i>		420	73	1	1.4%
<i>Dsec-attPpBac-A26</i>	<i>p(GP-JFRC7-20XUAS-IVS-GCaMP6s)</i>	355	41	1	2.4%
<i>Dsec-attPpBac-A79</i>	<i>pUAS-myrGFP, QUAS-mtdTomato(3xHA)</i>	265	27	0	0
<i>Dsec-attPpBac-A80</i>		249	26	0	0
<i>Dsec-attPpBac-A26</i>		260	32	0	0
<i>Dsec-attP1029</i>		483	26	0	0
<i>Dsec-attP2</i>		290	31	0	0
<i>Dsec-attP40</i>		210	28	1	3.5%
<i>Dsec-attP40 locus/sgRNAs</i>	CRISPR KI UAS-CD4-GFP	240	37	1	2.7%

Integration efficiencies (especially at *Dsec-attP2* and *Dsec-attPsu(Hw)attP2*) might be higher when aiming for integration of smaller constructs. For CRISPR-mediated integration at the *attP40* locus, a sgRNA expression vector *pCFD5-Dsec-attP40* and *Dsec-attP40-3xP3-DsRed-UAS-CD4:GFP* were co-injected.

Table S3. Summary of *attP* testing, related to Figure 1.

<i>attP</i> site	Comment
<i>Dsec-attP1029</i>	Marked by GFP expression in muscle; weaker Gal4 expression than same driver at <i>Dsec-attP40</i> ; used for direct integration of <i>10XUAS-FRT>STOP>FRT-myr::smGFP-FLAG</i> cassette via CRISPR/Cas9
<i>Dsec-attP40</i>	Marked by RFP expression in 3P3 pattern; strong Gal4 expression; used for direct integration of <i>10XUAS-FRT>STOP>FRT-myr::smGFP-HA</i> cassette via CRISPR/Cas9; UAS-CD4:GFP reporter with ectopic expression in mushroom body; highest integration efficiency of <i>pUAS-myrGFP</i> , <i>QUAS-mtdTomato(3xHA)</i> among tested sites
<i>Dsec-attP2</i>	Marked by very strong RFP expression in 3P3 pattern, no successful integration
<i>Dsec-attPpBac-A26</i>	Marked by RFP expression in 3P3 pattern; Split-Gal4 driver expression weaker than same driver at <i>Dsec-attPwhite</i> locus; reliable signal from UAS-constructs without ectopic expression
<i>Dsec-attPsu(Hw)attP2</i>	Marked by strong RFP expression in 3P3 pattern, no successful integration
<i>Dsec-attPJK22C</i>	Marked by strong RFP expression in 3P3 pattern, no successful integration, homozygous lethal
<i>Dsec-attPwhite</i>	Marked by RFP expression in 3P3 pattern; strong Split-Gal4 and broad enhancer-Gal4 expression; ectopic expression with restricted-Gal4 driver; strong signal from UAS-reporter with ectopic expression in optic lobes
<i>Dsec-attPpBac-A79</i>	Marked by RFP expression in 3P3 pattern, no successful integration
<i>Dsec-attPpBac-A80</i>	Marked by RFP expression in 3P3 pattern, no successful integration

Table S5. List of potential PN downstream neurons based on EM circuit data, related to Figure 4.

Name	neuprint ID	Type
LHPD4c1	421641859	lateral horn neuron
LHCENT6	5813068669	lateral horn neuron
LHCENT2	327499164	lateral horn neuron
MBON18	5813020828	mushroom body output neuron
NPFP1	1043117106	
LHAD3a2_a	360246734	lateral horn neuron
LHMB1	5813020988	lateral horn neuron
MBON24	487143497	mushroom body output neuron
SLP044_b	359555152	superior lateral protocerebrum neuron
SLP098	5813019807	superior lateral protocerebrum neuron
SLP098	5813019807	superior lateral protocerebrum neuron
SLP101	329582105	superior lateral protocerebrum neuron
SLP101	391630222	superior lateral protocerebrum neuron
SLP102	330303073	superior lateral protocerebrum neuron
SLP102	330640381	superior lateral protocerebrum neuron
SLP102	360315461	superior lateral protocerebrum neuron
SLP102	299272806	superior lateral protocerebrum neuron
SLP103	391599963	superior lateral protocerebrum neuron
SLP103	361964228	superior lateral protocerebrum neuron
SLP103	359900300	superior lateral protocerebrum neuron
SLP104	5813087454	superior lateral protocerebrum neuron
SLP104	329215304	superior lateral protocerebrum neuron
SLP104	327509674	superior lateral protocerebrum neuron
SLP105	297860627	superior lateral protocerebrum neuron
SLP105	297519843	superior lateral protocerebrum neuron
SLP105	328209735	superior lateral protocerebrum neuron
SLP106	326504486	superior lateral protocerebrum neuron
SLP106	327519295	superior lateral protocerebrum neuron
SLP107	296143923	superior lateral protocerebrum neuron
SLP107	325814784	superior lateral protocerebrum neuron
SLP108	325484974	superior lateral protocerebrum neuron
SLP113	390589591	superior lateral protocerebrum neuron
SLP138	451658249	superior lateral protocerebrum neuron
SLP193_a	421642764	superior lateral protocerebrum neuron
SLP205	296829531	superior lateral protocerebrum neuron
SLP328	391971839	superior lateral protocerebrum neuron
SIP006	328265281	superior intermediate protocerebrum neuron
SIP007	5813020789	superior intermediate protocerebrum neuron
SIP007	298935146	superior intermediate protocerebrum neuron
SIP007	298935146	superior intermediate protocerebrum neuron
SIP008	330989587	superior intermediate protocerebrum neuron
SIP008	359628017	superior intermediate protocerebrum neuron
SIP009	548562283	superior intermediate protocerebrum neuron
SIP009	518899771	superior intermediate protocerebrum neuron
SIP010	609587511	superior intermediate protocerebrum neuron
SIP010	609591989	superior intermediate protocerebrum neuron
SIP010	609591880	superior intermediate protocerebrum neuron

SIP011	609591758	superior intermediate protocerebrum neuron
SIP011	609591891	superior intermediate protocerebrum neuron
SIP011	609587594	superior intermediate protocerebrum neuron
SIP011	609591823	superior intermediate protocerebrum neuron
SIP012	607886496	superior intermediate protocerebrum neuron
SIP012	576864518	superior intermediate protocerebrum neuron
SIP013	5813104563	superior intermediate protocerebrum neuron
SIP013	609501640	superior intermediate protocerebrum neuron
SIP013	609591686	superior intermediate protocerebrum neuron
SIP013	577205852	superior intermediate protocerebrum neuron
SMP022	516857964	superior medial protocerebrum neuron
SMP022	640276971	superior medial protocerebrum neuron
SMP022	515092013	superior medial protocerebrum neuron
SMP023	579239039	superior medial protocerebrum neuron
SMP023	578919867	superior medial protocerebrum neuron
SMP024	609247082	superior medial protocerebrum neuron
SMP024	5813082780	superior medial protocerebrum neuron
SMP024	579260627	superior medial protocerebrum neuron
SMP024	5813019920	superior medial protocerebrum neuron
SMP024	735470305	superior medial protocerebrum neuron
SMP025	297572235	superior medial protocerebrum neuron
SMP025	266873401	superior medial protocerebrum neuron
SMP025	5813055768	superior medial protocerebrum neuron
SMP025	298245502	superior medial protocerebrum neuron
SMP025	267223104	superior medial protocerebrum neuron
SMP034	5813039860	superior medial protocerebrum neuron
SMP034	266191395	superior medial protocerebrum neuron
SMP549	329566197	superior medial protocerebrum neuron
CL017	544831533	superior clamp neuron
CL018	578587420	superior clamp neuron
CL018	548225503	superior clamp neuron
CL018	543412036	superior clamp neuron
CL018	574420970	superior clamp neuron
CL019_a	759633968	superior clamp neuron
CL019_b	5812981249	superior clamp neuron
CL019_b	543023799	superior clamp neuron
CL019_b	578587259	superior clamp neuron
CL020	542699260	superior clamp neuron
CL020	547551580	superior clamp neuron
LHAV6c1	544435277	lateral horn neuron
LHAV6c1	482732443	lateral horn neuron
LHAV6c1	548199677	lateral horn neuron
LHAV6c1	607212413	lateral horn neuron
LHAV6d1	5813067769	lateral horn neuron
LHAV6d1	609587618	lateral horn neuron
LHAV6d1	519249805	lateral horn neuron

Table S6. Oligonucleotides used to generate single sgRNA expression vectors.

Target	Forward primer (5'-3')	Reverse primer (5'-3')
<i>Dsec-attPJK22C sgRNA1</i>	GTCGCATCAGCAACGCACAGTGGG	AAACCCCACTGTGCGTTGCTGATG
<i>Dsec-attPJK22C sgRNA2</i>	GTCGACTGTGCGTTGCTGATGCAG	AAACCTGCATCAGCAACGCACAGT
<i>Dsec-attP2 sgRNA1</i>	GTCGGCGAATGGCGAAAGCTGCGC	AAACGCGCAGCTTTCGCCATTTCG

Table S7. Oligonucleotides used to generate multi-sgRNA expression vectors.

Target	Name	Sequence (5'-3')	Resulting sgRNAs
<i>Dsec-su(Hw)attP2</i>	<i>PCR1fwd</i>	GCGGCCCGGGTTCGATTCCCGGCCGATGCAGGAATCGC ACGGACGTGTCGGTTTTAGAGCTAGAAATAGCAAG	sgRNA1: GGAATCGCACGGACGTGTGCG
	<i>PCR1rev</i>	ATTTTAACTTGCTATTTCTAGCTCTAAAACGCAGATTCTCA CTTCATGCTTGCAACGACCGGGAATCGAACCC	sgRNA2: AGCATGAAGTGAGAATCTGCG
<i>Dsec-attP40</i>	<i>PCR1fwd</i>	GCGGCCCGGGTTCGATTCCCGGCCGATGCAGTTACACA GCCCTTGCTGGGTTTTAGAGCTAGAAATAGCAAG	sgRNA1: GTTACACAGCCCTTGCTGGTGG
	<i>PCR1rev</i>	ATTTTAACTTGCTATTTCTAGCTCTAAAACACACACATTGG GCAGCACAGTGCACGACCGCGGAATCGAACCC	sgRNA2: CTGTGCTGCCCAATGTGTGT
<i>Dsec-attP1029</i>	<i>PCR1fwd</i>	GCGGCCCGGGTTCGATTCCCGGCCGATGCATTAAAGTTA AACAAGCGGTAGTTTTAGAGCTAGAAATAGCAAG	sgRNA1: TTAAAGTTAAACAAGCGGTA
	<i>PCR1rev</i>	ATTTTAACTTGCTATTTCTAGCTCTAAAACCTTTCTACTTTCA GATTGTTTGCACGACCGCGGAATCGAACCC	sgRNA2: AACCAATCTGAAAGTAGAAA

Supplementary References

- S1. Stern, D. L. Transgenic tools for targeted chromosome rearrangements allow construction of balancer chromosomes in non-*melanogaster Drosophila* species. *G3 Genes|Genomes|Genetics* **12** (2022).
- S2. Markstein, M., Pitsouli, C., Villalta, C., Celniker, S. E. & Perrimon, N. Exploiting position effects and the gypsy retrovirus insulator to engineer precisely expressed transgenes. *Nat Genet* **40**, 476-483 (2008).
- S3. Pfeiffer, B. D. *et al.* Refinement of tools for targeted gene expression in *Drosophila*. *Genetics* **186**, 735- (2010).
- S4. Knapp, J. M., Chung, P. & Simpson, J. H. Generating customized transgene landing sites and multi-transgene arrays in *Drosophila* using phiC31 integrase. *Genetics* **199**, 919-934 (2015).
- S5. Ni, J. Q. *et al.* A *Drosophila* resource of transgenic RNAi lines for neurogenetics. *Genetics* **182**, 1089-1100 (2009)
- S6. Stern, D. L. *et al.* Genetic and transgenic reagents for *Drosophila simulans*, *D. mauritiana*, *D. yakuba*, *D. santomea*, and *D. virilis*. *G3 (Bethesda)* **7**, 1339-1347 (2017).
- S7. Takagi, S. *et al.* Olfactory sensory neuron population expansions influence projection neuron adaptation and enhance odour tracking. *Nat Commun* **15**, 7041 (2024)